Assessment of thermal stabilisation measures based on numerical simulations at a Swiss Alpine permafrost site

Elizaveta Sharaborova[1,2], Michael Lehning[1,2], Nander Wever[2], Marcia Phillips[2], and Hendrik Huwald[1,2]

[1]Environmental Engineering Institute, Laboratory of Cryospheric Sciences, Ecole Polytechnique Fédérale de Lausanne (EPFL) Valais/Wallis, Sion, Switzerland
[2]WSL Institute for Snow and Avalanche Research SLF, Davos, Switzerland

Correspondence: Elizaveta Sharaborova (elizaveta.sharaborova@epfl.ch)

Abstract. Global warming causes thawing of permafrost, leading to landscape changes and infrastructure damage, problems that have intensified worldwide in all permafrost regions. This study numerically investigates the impact of different thermal stabilisation methods on preventing or delaying permafrost thawing. To test different technical methods, an alpine mountain permafrost site with nearby infrastructure is investigated. Model simulations represent the one-dimensional effect of heat fluxes across the complex system of snow-ice-permafrost layers and the impact of passive and active cooling, including engineered energy flux dynamics at the surface. The results show the efficiency of different passive, active and combined thermal stabilisation methods in influencing heat transfer, temperature distribution, and the seasonal active layer thickness. Investigating each component of thermal stabilisation helps quantify the efficiency of each method and determine their optimal combination. Despite providing efficient cooling in winter, passive methods are less efficient, as the active layer thickness remains over 1 m. Conductive heat flux attenuation alone takes several years to form a stable frozen layer. Active cooling, when powered by solar energy, decreases the active layer thickness to only a few decimetres. The combination of active and passive cooling, together with conductive heat flux attenuation, performs best and allows excess energy to be fed into the local grid. The findings of this study show the evolution of ground temperature and permafrost at a representative alpine site under natural and thermally stabilised conditions, contributing to understanding the potential and limitations of stabilisation systems and formulating recommendations for optimal application.

1 Introduction

The effect of increasing air temperature on permafrost is the result of complex and interacting processes occurring in different layers, including the grain size of rocks, the snow cover, and the active layer. On the continental scale, between 2007 and 2016, the Arctic continuous permafrost experienced a warming of approximately 0.39 °C while the discontinuous permafrost warmed 0.20 °C (Biskaborn et al., 2019). In particular, this warming reached 0.8 °C per decade in the Svalbard archipelago and 0.5 °C per decade in Russia (Smith et al., 2022). In the same period, global mountain permafrost temperatures increased by 0.19 °C (Biskaborn et al., 2019; Etzelmüller et al., 2020), responding to the rise of the atmospheric 0 °C isotherm (Kenner et al., 2024). The general trend at some alpine mountain permafrost sites showed that warming at 10 m depth was 0.4 °C per decade between 1987 and 2009 (Haeberli and Gruber, 2009; Noetzli et al., 2024). These changes have led to an increase in

active layer thickness (ALT) and shifted latitudinal permafrost limits northward (Biskaborn et al., 2019; Smith et al., 2022) and elevation limits to higher altitudes (Kenner et al., 2024; Noetzli et al., 2024). In Sweden, Greenland, and Svalbard, the ALT has been increasing since the 1990s (Strand et al., 2021), and similarly in mountain permafrost, where it has doubled in parts of the Swiss Alps in the 21st century (Smith et al., 2022; Swiss Permafrost Monitoring Network (PERMOS), 2024; Noetzli et al., 2024). On the Schilthorn mountain (Bernese Alps, Switzerland), annual average ground temperatures increased from –0.5 to +0.03 °C, resulting in a tripling of the ALT (Hauck, 2002; Swiss Permafrost Monitoring Network (PERMOS), 2024), while at the Stockhorn borehole (Valais, Switzerland), a four-fold acceleration in warming led to a decadal rate of +0.64 °C between 2012 and 2022 (Morard et al., 2024). At the Murtèl–Corvatsch borehole (Grisons, Switzerland), the warming over 18 years (1987–2006) reached approximately 0.5 °C at 11.6 m depth and 0.3 °C at 21.6 m depth (Harris et al., 2009a), with continued increases over 35 years (1987–2022) from –1.8 °C to –1.0 °C at 15–20 m depth (Haeberli et al., 2023).

Thawing and warming permafrost and increasing ALT present a risk to infrastructure foundations. It has been estimated that almost 70% of infrastructure in the permafrost could be affected by 2050, with transport infrastructure (roads, railways, cable cars, etc.) being the most vulnerable and most abundant (Hjort et al., 2018, 2022). A prominent Arctic example of infrastructure impacted by permafrost changes is the runway of the international airport in Longyearbyen, Svalbard, where the thawing of ice-rich soils caused uneven settlement during the summer season, and the refreezing in the fall provoked heave formation, ultimately leading to the destruction of the runway (Instanes and Mjureke, 2005). Besides transport infrastructure, over 1'000 settlements, and over 9'000 km of pipelines are located in areas subject to permafrost risk (Hjort et al., 2022).

In mountain regions such as the Swiss Alps, permafrost thawing also causes significant impacts. Unlike Arctic areas, mountain permafrost in steep rock slopes contains little ice; its thawing allows water infiltration, which can lead to high pressures and rapid temperature increases. Infrastructure such as cable cars, houses, antennas and avalanche protection systems built on permafrost rock slopes can be destabilised (Duvillard et al., 2021). An impressive example is the 2017 Pizzo Cengalo rock avalanche in Bondo, Switzerland (Mergili et al., 2020), a cascading event involving rockfall, rock-ice avalanche, and debris flow (Walter et al., 2020). Such process chains are often linked to cryospheric changes such as glacial de-buttressing, retreating hanging glaciers, or thawing permafrost (Harris et al., 2009b; Haeberli et al., 2017). Ice-rich permafrost can also develop at the base of steep slopes in the snow avalanche and rockfall deposition zones (Kenner et al., 2019). Although these zones should be avoided in infrastructure planning (Bommer et al., 2010), this is not always possible. Ice warming and melting, combined with water infiltration, can lead to subsidence and creep, damaging the infrastructure on ice-rich ground.

All of these challenges, whether from new or intensifying natural hazards or from the difficulties of building on mountain permafrost, require technical adaptations. These include the use of flexible, adjustable, or semi-mobile structures, specially adapted building materials, and cooling techniques (Haeberli et al., 2010; Bommer et al., 2010). The search for solutions for stabilisation of permafrost substrates in the currently affected regions, above, below, or around critical infrastructures, and wherever new structures on permafrost are planned is becoming inevitable. Stabilisation of permafrost means primarily keeping it at sub-freezing temperatures and minimising the depth and dynamics of the ALT.

There are several thermal stabilisation and ground cooling methods applied worldwide, which can be divided into passive methods (requiring no external energy) and active methods (needing additional power supply). Passive systems typically

increase thermal resistance in the upper layers of the ground using solar reflectors and shields (Qin et al., 2020), thermal insulation (Luo et al., 2018), and additional protective layers to reduce the impact of net solar radiation, heat convection, and conduction (Yinfei et al., 2016) above, within, and around the affected surface. However, these methods usually lack long-term effectiveness. Recent research proposes insulating the ground in summer to prevent heat penetration and lifting insulation in winter for better cooling (Sharaborova and Loktionov, 2022). Other techniques are based on lowering the ground temperature, by seasonal in-depth cooling, (Cheng, 2005) to protect underground infrastructure (e.g. tunnels) (Zhang et al., 2017) and highway embankments (Tian et al., 2021). However, they still face risks of surface deformation and decreasing efficiency due to climate change, shorter winters, and shrinking frozen volumes.

Although active cooling methods have been significantly developed in recent years, they are expensive due to power demands, limiting widespread use. Some progress has been made using solar energy (photovoltaic, PV) for active cooling in permafrost regions (Hu et al., 2020), offering an economical solution for field refrigeration without relying on grid power. This method could be improved by implementing solar radiation shielding and applying efficient energy redistribution and use, with solar panels installed on embankments helping to achieve the combined effect of shielding from direct solar radiation and powering the cooling system (Asanov and Loktionov, 2018; Loktionov et al., 2019). The system uses subsurface pipes through which a cooling liquid circulates to create a sub-0°C thermal "barrier layer" that prevents heat from penetrating deeper into the ground. The barrier layer, introduced by Sharaborova et al. (2022a) and Loktionov et al. (2022), serves to shield the cold ground against the penetration of ambient heat, rather than cooling the large volumes of the ground at depth. To achieve this, the cooling pipes are placed parallel and close to the ground surface within the natural thawing layer. The effect of this method has been simulated for lowland permafrost (Loktionov et al., 2022) and experimentally tested (Sharaborova et al., 2022b).

Permafrost in mountain regions presents additional challenges due to settlement, deformation, and creep in complex ice-bearing terrain, requiring careful assessment and timely remedial measures to ensure the longevity of the infrastructure (Bommer et al., 2010). Special construction methods, such as flexible foundations for buildings subjected to deformation, can address subsidence and creep (Phillips et al., 2007; Harris et al., 2009a). Thermal stabilisation techniques, including insulation materials such as foam glass and extruded polystyrene, and passive cooling systems such as thermosyphons, are used in mountain permafrost construction, although thermosyphons are less common in the Alps (Phillips et al., 2007; Bommer et al., 2010).

To test and estimate the effect of thermal stabilisation methods on-site, experiments and monitoring are required. However, experimental designs are time-consuming and expensive. Modelling using numerical simulations is a good alternative to examine the impact and performance of cooling methods and to provide a better understanding of the thermal changes that occur in the permafrost. Different models are used to simulate permafrost. Established physics-based 1D models such as the Coup-Model (Jansson and Karlberg, 2004; Marmy et al., 2013; Schaefer et al., 2014; Marmy et al., 2016), SNOWPACK (Lehning et al., 1999a) and CryoGrid (Westermann et al., 2023) are used to simulate mass and energy exchange processes in the soil-snow-atmosphere system. Such models have also been extended to cover wider areas as distributed 1D columns, for instance, in Alpine3D, which is based on the SNOWPACK model (Haberkorn et al., 2017) or a recent update of GERM (Huss et al., 2008; Farinotti et al., 2012) with a permafrost module (Pruessner et al., 2021). These models can also be used to simulate protective insulation methods. An example is the SNOWPACK simulation of partial glacier protection using a geotextile cover

95 (Olefs and Lehning, 2010) or the assessment of snow farming (Grünewald et al., 2018) that allows us to examine in detail the energy exchange between different layers. Another example is the use of the 3D finite element method (FEM) package, specifically developed for permafrost ground calculations (Alekseev et al., 2018), to gauge the effectiveness of a thermal stabilisation method in permafrost (Loktionov et al., 2022).

The present study uses the SNOWPACK model to investigate the processes that occur in the permafrost during the application 100 of passive and active thermal stabilisation methods at a selected mountain permafrost site. Principal objectives are (1) to numerically examine the heat flux distribution in complex snow–ice–permafrost substrates and at the interface with thermal stabilisation systems and (2) to quantify the impact of thermal stabilisation on the ALT. We investigate how various cooling methods affect the long-term evolution of permafrost and its preservation in a cold state, and how they influence the thickness of the active layer, in combination with thermal stabilisation approaches. The results are expected to help assess the pros and 105 cons of different thermal stabilisation methods for protection and preservation of permafrost. The numerical studies allow the creation of an integrated view of the technology behaviour and help to adapt it for in-situ application.

The objective of this study is the numerical evaluation of the performance of engineering methods for thermal stabilisation of alpine permafrost and its sensitivity to different design parameters. The study uses data from the Schilthorn Mountain borehole, Switzerland, a high-elevation site representative of alpine permafrost regions. By analysing their impact on key variables 110 such as ground temperature, heat fluxes, and ALT, we aim to provide information on the efficacy of these measures and their potential to improve the resilience of permafrost against atmospheric warming. The findings contribute to optimising engineering practices in permafrost regions and addressing knowledge gaps in permafrost thermal management. The results obtained are specific for the particular site conditions at Schilthorn, because parameter selection was carried out to best reproduce the measured temperature profile evolution for the natural situation. However, results can be considered representative for a range 115 of conditions typical of alpine permafrost. Furthermore, research on mountain permafrost stabilisation remains limited. As a result, this study offers new insights, but also highlights the need for further research to make wider comparisons and draw broader conclusions.

2   Modelling with SNOWPACK

Here, we build on previous research employing the SNOWPACK model for permafrost studies (Luethi et al., 2017; Pruessner 120 et al., 2018, 2021). Initially, the model was developed for avalanche warning (Lehning et al., 2000) and computes 1D heat transfer, water transport, vapour diffusion, and mechanical deformation, including new snow, wind drift, and snow ablation. It describes the layers of the ground (Luetschg et al., 2008) where the physical properties (thermal conductivity, heat capacity, density) remain constant over time (Pruessner et al., 2021). SNOWPACK offers both a simple bucket water transport model (Lütschg, 2005) and an advanced Richards water transport model (Wever et al., 2014, 2015) to simulate the transfer of water 125 from the snow cover to the underlying substrate. In the current study, we use the bucket scheme, which allows us to directly specify the fixed substrate volumetric content for each soil layer. In contrast, the Richards scheme requires specifying the grain size of the ground layers to determine the water retention properties of the soil. The SNOWPACK bucket model is computa-

tionally very efficient and was tested for various mountain permafrost sites. SNOWPACK also allows for the incorporation of artificial materials on the surface as an additional model layer. This feature has been used to successfully model geotextile-
130 covered snow (Olefs and Lehning, 2010), showing good agreement between the modelled and observed temperature profile of artificially conserved snow. This feature of the model is also used in the present work to represent the inclusion of thermal insulation material.

Heat sinks and sources can be represented in the model by an advective heat flux formulation (Luethi et al., 2017). This capability can be used to heat or cool any layer, including the ground, and model, for example, talik formation in the permafrost
135 (Luethi et al., 2017). Based on these previous applications of SNOWPACK, the model is considered to be well suitable for studying the effects of thermal stabilisation systems in mountain permafrost. In this study, we used SNOWPACK Version 3.7 to model the effects of cooling pipes in the ground. We introduced an optional feature to the model to allow for a representation of the artificial cooling as if it were installed on the site, and to control heat transfer between the ground and the cooling pipes. The modified version of the model includes a switch to regulate temperature and to remove heat from the ground by activating
140 the advective heat mode. Upper and lower temperature limits can be specified. When the ground temperature has cooled to the set threshold, the cooling system is turned off. If the ground temperature passes the specified upper limit, the cooling is activated again.

The decision to use SNOWPACK to model thermal stabilisation in permafrost, in contrast to previous work by Loktionov et al. (2022), is motivated by its representation of snow dynamics, ground thermal properties, and permafrost temperature evo-
145 lution over the full simulation period. In Loktionov et al. (2022) a 3D model uses a type III boundary condition, which can be beneficial for permafrost modelling but relies on a simplified treatment of surface processes. The model used by Loktionov et al. (2022) is more practical for engineering reasons, especially when the ground is under the thermal influence of the infras-tructure and constructions. SNOWPACK is more aligned with scientific research goals, given its comprehensive treatment of snow and soil physics. The advantage of SNOWPACK is that it presents a full set of surface fluxes, including a wide choice of
150 stability corrections. This approach allows the surface temperature to evolve naturally based on the energy balance and the ap-plied cooling methods. These boundary conditions provide an accurate representation of the heat exchange between the ground and the atmosphere, with a representation of the heat flux at the soil-atmosphere interface. This is especially advantageous when measured surface temperatures are unavailable or unreliable. Moreover, the 3D model comes with higher computational demands, which can limit its practicality for multi-year simulations or sensitivity analyses. In comparison, SNOWPACK en-
155 ables the rapid simulation of long periods with detailed vertical resolution, making it more suitable for exploring a range of scenarios and parameter sensitivities. SNOWPACK enables the detailed representation of every model layer including temper-ature, heat flux, and the possibility of monitoring the output of the permafrost parameters (ground temperatures, volumetric water content, bulk density, thermal conductivity, heat capacity, temperature gradient, etc.). Another notable difference lies in the treatment of the snow cover. SNOWPACK can simulate the evolution of the snow cover either by prescribing measured
160 snow height values or by calculating the new snow depth based on observed precipitation and air temperature. When the snow cover is prescribed from measured snow depth values it takes into account local drifting snow, since that is included in the snow depth measurements. The 3D model of Loktionov et al. (2022) uses a constant albedo value for snow, suggesting a simplified

representation. SNOWPACK includes a physically based multi-layer snow model, simulating snow accumulation, compaction, metamorphism, and albedo evolution. This more realistic snow treatment is critical in permafrost studies, as snow insulation is a dominant control on ground thermal regimes. SNOWPACK fits the goals of this study because it matches the available data, offers clear transparency, accurately represents snow processes, and runs efficiently.

3 Description of study site and data

In this study, we used the temperature data from the Schilthorn PERMOS permafrost borehole site, canton Bern, Switzerland (46.558292 N, 7.834626 E, 2923 m a.s.l.) (Swiss Permafrost Monitoring Network (PERMOS), 2024). We selected this site because it is representative of many alpine permafrost locations and because the nearby infrastructure could be affected by permafrost thaw. During the past decade, the ALT at this site has doubled (Hauck and Hilbich, 2024). Hauck and Hilbich (2024) indicating a general deepening of ALT from 4–5 m before 2008 to 5–7 m by 2016, with subsequent increases leading to 13 m after the extremely hot summer of 2022. This approaches the threshold (about 14 m) beyond which full winter refreezing may no longer be possible. The ALT thickening causes direct challenges for the infrastructure, such as local cable car foundations, pylons, and buildings. The thaw of the permafrost can cause slope instabilities, rockfalls, or subsidence, destabilising building foundations, particularly when located on steep slopes. These risks are also applicable to similar Alpine sites with cable car infrastructure or other facilities, for example, the Zermatt / Matterhorn area in Switzerland (Weber et al., 2017), or the Chamonix/Mont Blanc region in France (Duvillard et al., 2021).

Figure 1 shows the location of the site with respect to the spatial distribution of permafrost, indicating ground temperatures and ice content, and average yearly totals of solar radiation. Meteorological stations and borehole sites (Table 1) are shown in Figure 1 on the right panel. The observational permafrost temperature and atmospheric data sets of this site are well suited for modelling purposes, as they include sufficiently long periods of meteorological forcing and permafrost temperature and distribution.
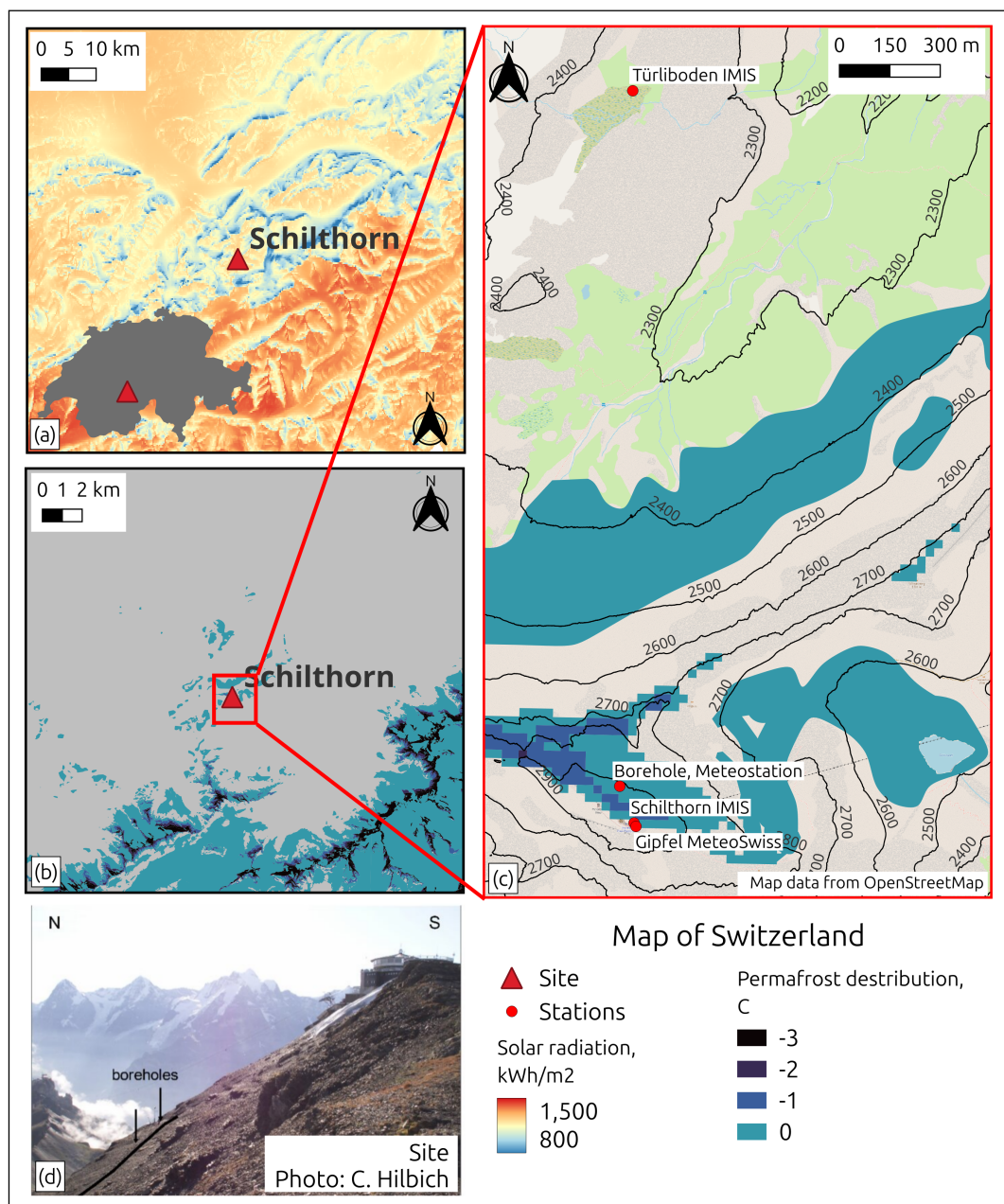
Figure 1. (a) Average yearly totals of solar radiation (Solargis, 2020) showing the Schilthorn site on an area map and on a map of Switzerland (gray shaded), (b) permafrost distribution adapted from Kenner (2018), (c) zoom into panel (b) indicating the site of Schilthorn borehole and surrounding meteorological stations Table 1, and (d) picture of borehole site and Schilthorn summit (Hilbich, 2010). Coordinates are based on UTM Zone 32T (EPSG:32632) for Switzerland. Schilthorn, E: 419500, N: 5158000. The map was generated using data from OpenStreetMap contributors and visualized in QGIS Development Team (2023).

Table 1. Meteorological and borehole data used for modelling. IMIS denotes Intercantonal Measurement and Information System.

Station	Coordinates	Data used
Schilthorn borehole (Swiss Permafrost Monitoring Network (PERMOS), 2024)	46.558 N, 7.835 E 2900 m a.s.l.	Borehole temperatures at depths (m): 0.2, 0.4, 0.8, 1.2, 1.6, 2, 2.5, 3, 3.5, 4, 5, 7, 9, 10, 11, 13
Schilthorn meteo station (Hoelzle et al., 2022; Swiss Permafrost Monitoring Network (PERMOS) and Hoelzle, 2021)	46.558 N, 7.835 E 2900 m a.s.l.	Air and surface temperature, relative humidity, wind speed, radiation (all components), snow depth
Schilthorn IMIS	46.557 N, 7.835 E 2996 m a.s.l.	Air temperature, wind speed, relative humidity
Türliboden IMIS	46.577 N, 7.835 E 2332 m a.s.l.	Reflected short-wave radiation, surface temperature, snow height, precipitation
Gipfel MeteoSwiss	46.557 N, 7.835 E 2970 m a.s.l.	Wind speed

The borehole temperatures were obtained from the Schilthorn SCH_5198 borehole operated by PERMOS (Swiss Permafrost
Monitoring Network (PERMOS), 2024). The borehole was established in 1998, it is 13 m deep and temperature is presently still
measured. The ground temperature averaged over 13 m depth and over the period 1998 to 2025 is 0.02 °C (Swiss Permafrost
Monitoring Network (PERMOS), 2024), the temperature range at the profile base is from -0.88 °C to 0.58 °C, and the ALT
changes from 4.4 m to 13 m. For simulations, we used atmospheric data (Table 1) from the PERMOS meteorological station
next to the borehole for the years 2000 to 2017 (Swiss Permafrost Monitoring Network (PERMOS) and Hoelzle, 2021; Hoelzle
et al., 2022). Long-term observations Hoelzle et al. (2022) state that the mean air temperature observed at Schilthorn (1998-
2018) is -2.60 °C, the mean snow height – 0.87 m, and the snow season usually lasts from October to June (Swiss Permafrost
Monitoring Network (PERMOS) and Hoelzle, 2021). Due to the presence of gaps, the data were completed with data from the
closest stations of the Intercantonal Measurement and Information System (IMIS) and MeteoSwiss network (Table 1) for the
same time period. To reduce bias related to the input data used, correlations between the Schilthorn meteorological station and
the other stations were calculated, and existing gaps were filled based on the regression coefficients obtained. The remaining
gaps were filled using the MeteoIO data generation and interpolation functions (Bavay and Egger, 2014).

We set up the model using the following set of parameters: volumetric ice, water, substrate, and voids content of the ground,
substrate density, thermal conductivity, and heat capacity. Based on the available data from the borehole temperature measure-
ments and previous modelling experience (Marmy et al., 2013; Ekici et al., 2015; Wagner et al., 2019; Hoelzle et al., 2022), we
use the substrate parameters listed in Table 2. The site is free of vegetation and the substrate consists of dark, deeply weathered
limestone on the surface of mainly sandy and gravel debris of several metres in depth, lying over strongly jointed bedrock

(Zappone and Kissling, 2021). The initial conditions required for the model were chosen to represent rocky ground, without specifying particular grain sizes for different layers. SNOWPACK requires appropriate initialisation; however, a spin-up may not be necessary if the ground temperature profile is initialised using the corresponding observational data. Each layer was divided into grid cells with a vertical extent of 0.1 m. The upper layer consists of well-drained loose rock (talus) and thus has a lower water content and moderate porosity, which explains the lower heat capacity required to reproduce the temperature distribution. Below this, the heat capacity increases representing the presence of an active layer, which is indicated by long spring and autumn zero-curtains (Swiss Permafrost Monitoring Network (PERMOS), 2024). The zero-curtain effect occurs as a result of the latent heat release/consumption during the phase transition (thawing or freezing) in the active layer. At this time, the ground temperature remains close to 0 °C over an extended period, while the air temperature may vary significantly. At depth, the standard values for limestone are used. The values for density and thermal conductivity are determined according to the given substrate stratification. The geological map (Zappone and Kissling, 2021) indicates that the site has a limestone bedrock at depth, with sandy and gravel debris in the upper layers. This justifies the use of the recommended corresponding values for this type of ground (Table 2).

Table 2. Parameters of geological substrate for the Schilthorn site simulations.

Depth, m	Volumetric content (ice, water, void, substrate), %	Density, $\mathrm{kg\,m^{-3}}$	Thermal conductivity, $\mathrm{W\,m^{-1}\,K^{-1}}$	Heat capacity, $\mathrm{J\,kg^{-1}\,K^{-1}}$
0-2.5	0; 20; 21; 59	1600	2.2	700
2.5-5	5; 20; 6; 69	2000	2.7	1000
5-13	10; 0; 0; 90	2700	3.0	900

4 Model simulations

To understand the processes that occur in permafrost soils, different configurations of numerical simulations were employed, first simulating natural conditions without modifications and then applying different thermal stabilisation methods. These simulations are numbered for easy reference and summarised in Table 3. The simulations have been run for the period June 2000 to January 2017. This time frame was selected as it precedes the significant observed increase in ALT, aligns with available meteorological data, and represents long-term observations of permafrost temperatures at the site. Focusing on the period before the major increase in ALT provides a baseline reference and highlights how early intervention could have prevented subsequent degradation, serving as a cautionary example for similar at-risk sites. Starting simulations in June avoids defining an initial snow cover and related uncertainties in its properties. The simulation of this period allows reconstructing the impact from thermal stabilisation methods and analysing the re-establishment of new temperature equilibrium within the ground, while preserving permafrost and delaying an increase in ALT at the site. This also allows to extrapolate obtained results to other similar permafrost sites. The model runs at an hourly time interval using meteorological forcing at 2 m above ground. This is

a temporal resolution necessary to represent fast-changing weather conditions and to simulate their impacts, for instance, on the energy balance and its various heat fluxes. For coherence, the model uses the same 1-hour time step. Internally, the model interpolates the hourly forcing on a 15-minutes time step (accomplished by the MeteoIO library (Bavay and Egger, 2014)) to avoid abrupt step changes and to obtain higher temporal resolution simulations.

Table 3. Overview of model simulations.

Exp.#	Description of model configuration
1	Natural conditions (reference case)
2	Shading of the surface by solar panels
	2.1 Shading from wind (wind speed decreased by 70%)
	2.2 Shading from liquid precipitation (liquid precipitation is neglected)
	2.3 Shading from snow (snow is neglected)
	2.4 Shading from direct short-wave radiation (direct short-wave radiation is neglected)
	2.5 Net effect of 'shading' (all parameters from 2.1-2.4 participate)
3	Thermal insulation at the surface throughout the year
4	Seasonal thermal insulation (heat flux attenuation during summer)
5	Active cooling (cooling pipes alone)
6	Active and passive cooling (cooling pipes and shading)
7	Active and passive cooling (cooling pipes and shading), 50% of PV power for cooling
8	Active and passive cooling (pipes and shading), 10% of PV power, seasonal thermal insulation

4.1 Natural conditions

Numerical simulations of natural conditions were carried out as a reference case (Exp. #1, Table 3) to evaluate the performance of the model compared to the measured temperatures from the borehole. These simulations, combined with the study of the modelled and measured substrate parameters at this site (Pellet et al., 2016; Scherler et al., 2010; Marmy et al., 2016), allowed the right setting to optimise the agreement of the modelled temperature distribution and the measured temperature data from the borehole. The soil albedo was set to 0.15 and we used the snow parametrisation of Schmucki et al. (2014), which estimates the albedo based on the time elapsed since the last snowfall, grain size and liquid water content (Lehning et al., 2002). The roughness length was set to 0.05 m accounting for the rocky surface. We used the Holtslag and Bruin (1988) correction model for atmospheric stability, which shows good performance on snow surfaces (Schlögl et al., 2017). We forced the model with available snow depth measurements from the site, avoiding the calculation of snow depth from precipitation data (Table 1) which includes only rainfall. In this way, we implicitly take into account local snow drift, since its effect is integrated in the observed snow depth. We force the model with incoming short-wave radiation, while the other energy balance components are computed by the model based on available meteorological forcing data (air temperature, wind speed, relative humidity, snow depth, and liquid precipitation equivalent) as well as the temperature at the base of the model domain for a full energy balance

assessment. At the surface, a Neumann boundary condition has thus been applied. The observed surface temperature data (Table 1) are not used directly as input for the model simulations, but serve to compare the model output with the measurements as a consistency check. At the base of the model domain, a Dirichlet boundary condition is used, prescribing borehole temperature measurements ranging from -0.9 °C to -0.1 °C.

250   We quantitatively compared the model output with the borehole temperature measurements using standard statistical analysis such as bias, root mean square error (RMSE) and correlation (Pearson coefficient) at different depths for monthly mean averages and for the whole time series. In addition, we compared the mean values and standard deviations for different model setups with observations. The setup that produced the best performance was chosen as a reference case (Exp. #1).

4.2   Thermal stabilisation modelling experiments

255   ### 4.2.1   Shading of the surface

Surface shading from structures above the ground protects the soil from direct solar radiation, snow, and liquid precipitation. It also affects the wind speed near the ground. We simulate the shading of solar panels placed above the ground, exceeding the height of the snow cover, as proposed by Loktionov et al. (2022). To quantify the impact of shading of various parameters individually and in combination, we conducted experiments in two stages. In the first stage, we investigated the effect of

260   each of the following parameters independently of each other: (1) wind speed decreased by 70%; (2) the ground completely protected from snow and liquid precipitation; (3) only the diffuse component of incident short-wave radiation, which is derived from the reference case SNOWPACK simulation under natural conditions. In a second step, all parameters were modified simultaneously, simulating the combined effect on heat transfer and vertical temperature distribution.

     Snow accumulation works as natural insulation; therefore, in winter it prevents heat loss from the ground and limits natural

265   cooling (Wang et al., 2019). Liquid precipitation has a negative impact as it increases the ALT which accelerates permafrost degradation (Zhu et al., 2017; Wang et al., 2021). Changes in wind speed can have a positive or negative impact on permafrost, affecting heat transfer, snow re-distribution and moisture content, which in turn can slow or accelerate permafrost degradation (Zhao and Yang, 2022). Based on these known impacts, we designed our simulations to test the effect of neglecting individual components: wind, solid and liquid precipitation, and direct solar radiation to better understand their respective roles in

270   permafrost thermal dynamics.

     The choice of parameters (1) and (2) was based on previous modelling results investigating thermal stabilisation (Loktionov et al., 2022). However, Loktionov et al. (2022) instead applied a solar radiation value that was decreased by 95% from global horizontal irradiance (GHI). In the present study, we can revert to the modelled components of direct and diffuse solar radiation. Using only the diffuse solar radiation component is a simplified and idealised case, which allows to reproduce the effect of the

275   solar panels on ground temperature distribution, without applying an additional empirical coefficient. Removal of the direct solar radiation component accordingly reduced the radiative heat flux from the atmosphere (Liu and Jordan, 1960; Olson and Rupper, 2019; Li et al., 2020). In reality, solar panels may have a different impact on the solar radiation reaching the ground beneath solar panels depending on the spacing and inclination of the panels. The numerical tests with these assumptions allow

us to model the impact of the solar panels placed above the ground; however, for more accurate analysis, in situ experiments
280   are required. The test results will show the impact of each change on thermal stabilisation and its efficiency over the seasons.

4.2.2   Thermal insulation

We also model the ground covered with thermal insulation material. We simulate the presence of a 50-100 mm thick polystyrene
slab with a thermal conductivity of $0.033 \, \mathrm{W \, m^{-1} \, K^{-1}}$, a density of $28 \, \mathrm{kg \, m^{-3}}$ and a heat capacity of $1500 \, \mathrm{J \, kg^{-1} \, K^{-1}}$ to reduce
heat transfer from the atmosphere to the ground (Loktionov et al., 2022). The thickness range was chosen such that efficient heat
285   control in the context of this study was possible. We also simulated a thinner slab, which was found to be insufficient to reduce
heat transfer. The insulation material also increases the surface albedo. In the model, this was implemented as an additional
layer (styrofoam) at the top of the soil to preserve low temperatures at depth. Similarly to the ground layers (Section 3), the
thermal insulation layer and layers between 0 m and 0.2 m were divided into grid cells of 0.05 m for both 50 mm and 100 mm
material thickness. The albedo of the insulation material is set at 0.7, representative of white styrofoam with a high-albedo
290   reflective coating (Ramamurthy et al., 2015; Qiu et al., 2018; Chen et al., 2020) and similar to a snow cover. Two particular
cases are investigated: (1) insulation present all year round and (2) insulation present from the beginning of June until the end
of October (under snow-free conditions) and lifted from November until the end of May to allow the natural cooling process.
In (1), the insulating material protects the ground from direct contact with snow and rain. However, both types of precipitation
accumulate on top of the protection layer, which is considered in the simulation. The objective of (2) is to regulate the heat flux
295   (Sharaborova and Loktionov, 2022) by shielding during summer and favouring natural cooling in winter. The advantage of (2)
is the combination of the shading effect of the solar panels (Section 5.2.1) with the ground insulation material. This approach
has been introduced in the description of the method (Sharaborova and Loktionov, 2022) and is related to the attenuation of
the conductive heat flux and temperature. In this configuration, heat flux attenuation and prevention of permafrost thawing are
achieved without an external power supply. The method stabilises frozen ground by insulating the soil in warm seasons by
300   protecting the ground from solar radiation and precipitation, and by limiting convective heat transfer. Elevating the insulation
above snow cover in winter helps to use natural air circulation for cooling.

4.2.3   Thermal stabilisation with active cooling

This experiment (Exp. #5, Table 3) simulates the case of thermal stabilisation using a solar-powered heat pump (Sharaborova
et al., 2022a). The system combines the previously described passive protection (Section 4.2.1), where solar panels act as
305   sunscreens and as a power source for the heat pump cooling the ground through cooling pipes. The latter are modelled by
implementing a sink term at the level of the pipes that corresponds to the energy supplied by the solar panels keeping the
ground temperatures around the pipes below $0 \, °\mathrm{C}$.

   Similarly to previous studies simulating the application of a thermal stabilisation system (Loktionov et al., 2022), we model
cooling pipes applying a negative advective heat (q_{adv}) in the layers concerned. The advective heat is implemented in the
310   following way: First, the energy obtained from the solar panel is calculated using incoming short-wave radiation (ISWR),
the solar panel surface area ($A = 1 \, \mathrm{m^2}$), and the photovoltaic conversion efficiency ($\eta = 10\%$), as detailed in Equation (1).

Then, this power is applied to cooling, using the cooling energy efficiency rate (EER), Equation (1), which is related to the coefficient of performance (COP) for cooling machines and for heat pumps, according to Equation (2), and depends on the ambient (atmospheric) temperature. Equation (1) is adapted from Loktionov et al. (2022), the coefficients are specific to the equipment used. Finally, to determine the advective heat applied in the model, the cooling capacity is divided by the volume of the layer that contains the cooling pipes. This procedure is described using the following equations:

$$q_{\text{adv. heat}} = \frac{\text{ISWR} \cdot \eta \cdot A \cdot \text{EER}}{V} \tag{1}$$

$$\text{EER} = 4.8 - 0.12 \cdot T_a \tag{2}$$

$$\text{EER} = \text{COP} - 1 \tag{3}$$

Advective cooling was applied for the months of April to October. The cooling pipes are integrated into the model in a layer from 20 cm to 22.5 cm (the diameter of the pipe is 25 mm), cooling this layer to a minimum temperature of $-7.5\,^\circ$C, which corresponds to the mean temperature of the coolant circulating in the pipes (Loktionov et al., 2024a). To accurately represent this process, the grid cell thickness for layers between 0 m and 0.8 m was refined to 0.005 m. Active cooling from pipes creates a thermal barrier layer of a cold (frozen) slab inside the ground that protects the permafrost in summer from heat conducted from the surface deeper into the ground. Exp. #5 (Table 3) applies active cooling alone without shading the soil with solar panels. Exp. #6 (Table 3) combines passive and active cooling. In both experiments, the cooled area corresponds exactly to the area of the solar panels. However, in real life, this relation will be more complex, depending on the time of day, local topography, ground parameters, etc. Later in this study, we also examine cases in which only a portion of the energy from solar panels is reserved for cooling (Section 5.3).

5 Results and discussion

5.1 Natural conditions

The simulated evolution of ground temperature and observed snow depth at the Schilthorn site is shown in Figure 2 for the observation period from 2000 to 2017. By studying Schilthorn during a period when the ALT was thinner and before significant changes occurred, we gain valuable insights into the dynamics of mountain permafrost. The seasonal ALT is indicated by the $0\,^\circ$C isotherm and the temperature at the base of the model domain corresponds to the measured permafrost temperature in the borehole. We also observed an increase in ALT over the years from about 5 m to almost 7 m. In natural conditions, a realistic computation of the ground heat flux depends on an accurate representation of the snow depth as shown in Figure A1, where the modelled and measured snow align closely for most winters. For some periods, the measured snow depth is below the simulated, indicating that the model underestimates compaction, melt, and erosion (Lehning et al., 1999b). Figure 3a indicates that the modelled temperatures are slightly higher than measured. However, the monthly average difference for the entire simulation period never exceeds 1 $^\circ$C. Figure 3b indicates that the model and the observations are comparable with similar

long-term mean temperatures and standard deviations throughout the vertical profile, evidenced by correlation coefficients greater than 0.8, except for the middle layers, especially at depth around 5 m, where the coefficient drops to almost 0.6. This depth corresponds to the ALT, where even small temperature variations (on the order of a tenth of a degree) can cause significant fluctuations in its position (Marmy et al., 2016).
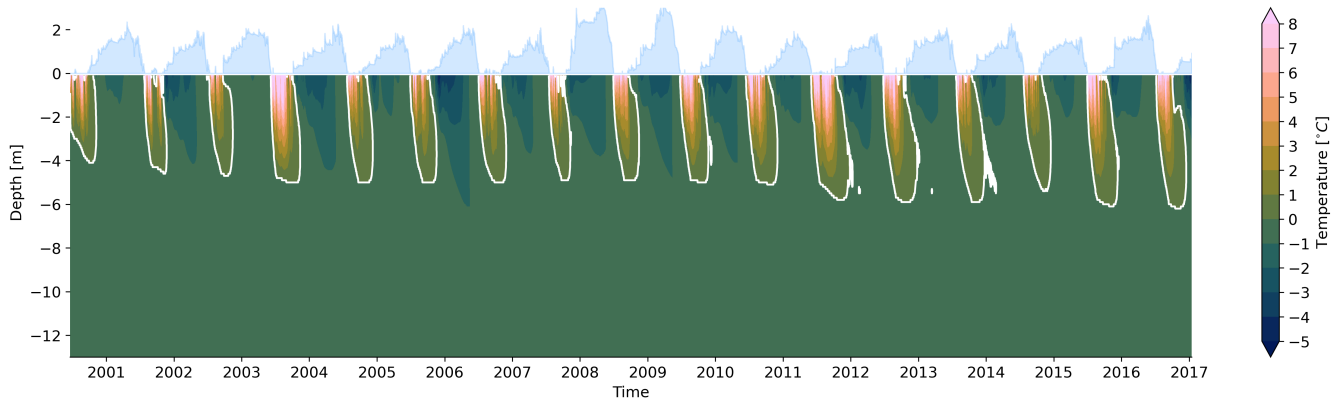
Figure 2. Time series of daily averaged modelled ground temperatures during natural undisturbed conditions at the Schilthorn site from 2000 to 2017. White contours indicate the 0 °C isotherm, i.e, the ALT. Snow depth is indicated in light blue above the 0 m depth level.
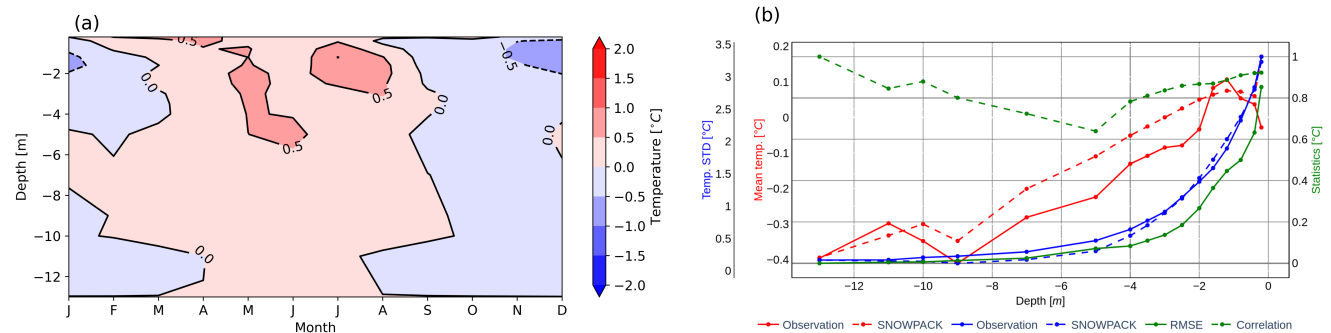
Figure 3. Comparison between modelled and measured ground temperatures at the Schilthorn site from 2000 to 2017. (a) Monthly averaged differences. Red (blue) colours indicate model temperature higher (lower) than observations. (b) Statistical analysis of the ground temperature differences averaged over the 17 years period. The 3 vertical axes represent: mean temperature (red), standard deviation (blue), other statistics (green). The horizontal axis indicates depth.

5.2 Thermal stabilisation experiments

5.2.1 Shading of the surface

We studied the impact of shading on the ground temperature in several experiments, isolating the effect of individual elements as described in Section 4.2.1 and comparing the simulations with the averaged natural conditions (Figure A2) as described
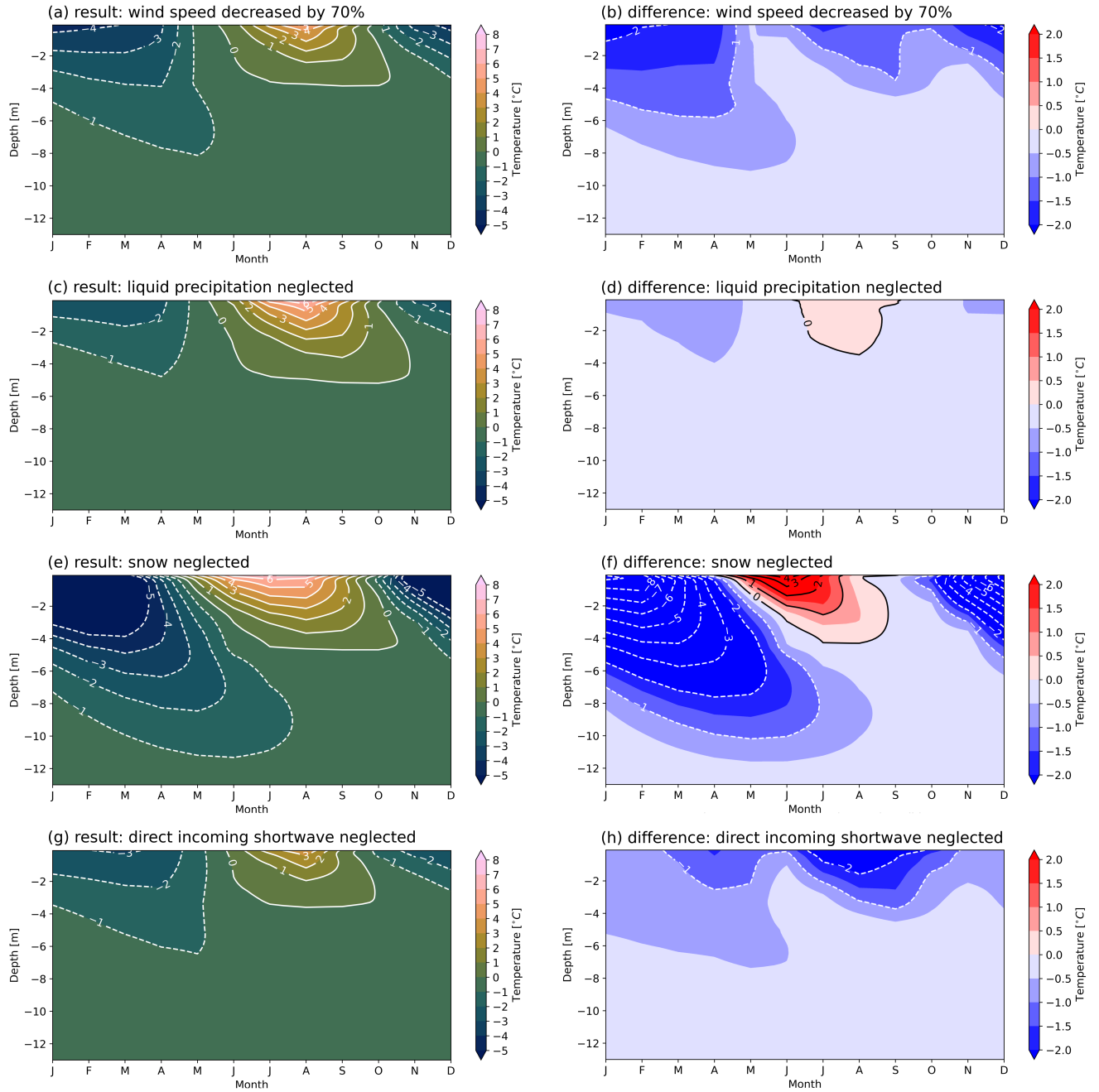
Figure 4. Monthly averaged modelled ground temperatures at the Schilthorn site from 2000 to 2017 resulting from individual model configurations defined in the 'shading' experiment (Exp. #2, Table 3). Panels (a, c, e, g): simulated ground temperature, panels (b, d, f, h): difference between simulated and natural conditions. Red (blue) colours indicate model temperature higher (lower) than observations. Experiments shown: (a, b) - wind speed reduced by 70% (Exp. #2.1); (c, d) - liquid precipitation set equal to zero (Exp. #2.2); (e, f) - snow depth set equal to zero (Exp. #2.3); (g, h) - direct component of incoming short-wave radiation neglected (Exp. #2.4).

above. Reduction of liquid precipitation by sheltering effects results in the smallest temperature changes in the ground (Figures 4d). The absence of liquid precipitation results in better cooling in winter and leads to a reduction in ALT thickness. Lower wind speed results in more efficient cooling for the full year (Figure 4a,b) as a result of changes in sensible heat fluxes on the surface. The greatest effect is seen when the natural isolating snow cover is absent (Figures 4e,f). This change results in a notable cooling of the ground in winter that supports the preservation of permafrost (Figure 4e). However, temperatures in summer increase because snow cover does not protect the ground from heat exposure and the favourable albedo effect is missing. If no snow is accumulated, the benefit of natural insulation is lost and the warming of the ground starts earlier than otherwise (Figure 4f). Heat loss during winter is not enough to compensate for the absence of snow. Finally, shading the ground from direct short-wave radiation (Figures 4g,h) results in lower ground temperatures in winter and, especially, in the summer season. This occurs because the incident radiative energy does not reach the ground and, as a result, the ALT (0 °C) is smaller.
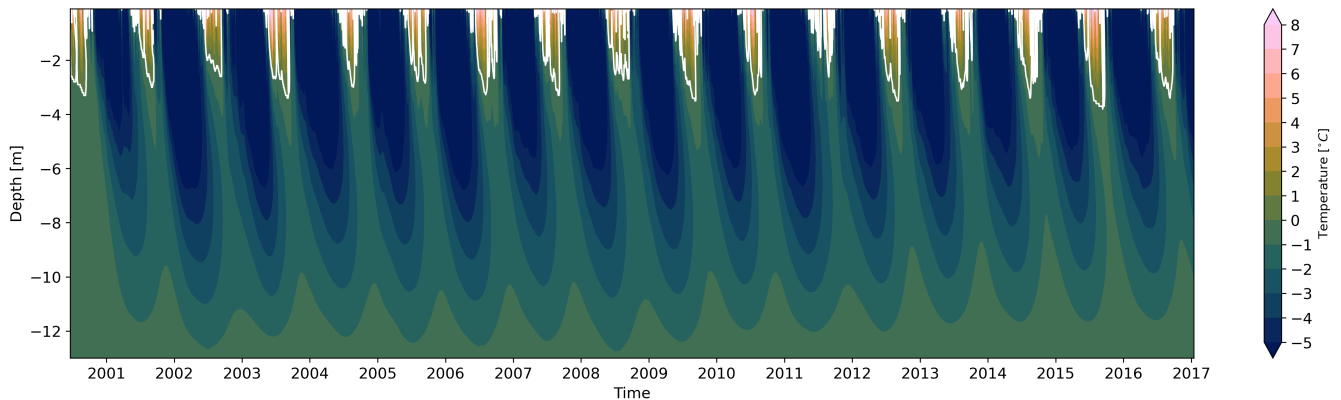
Figure 5. Time series of daily averaged modelled ground temperatures presenting the net effect of the 'shading' experiment (Exp. #2.5, Table 3) at the Schilthorn site for the period of 2000 to 2017. White contours indicate the 0 °C isotherm, i.e., the ALT.

In Figure 5 the net effect of shading at Schilthorn is shown, demonstrating that shading leads to cooling of the ground during winter and a decrease in ALT (depicted as the 0 °C isotherm in both figures). In agreement with the results by Quinton et al. (2011) testing different shading devices and observing the ground temperature decreasing with time, we also find a decreasing trend in ground temperature in our simulation results. However, there is still enough heat input to keep the ALT at a depth of several metres (Table D1). This indicates that this stabilisation method is insufficient and needs to be supplemented by other elements described by Cheng (2005) and Loktionov et al. (2022). In contrast, the method amplifies the annual cycle of thawing and refreezing. In the long-term trend (Figure 5), the net effect of this method allows rapid ground cooling every winter, however, it does not create and maintain a thermal barrier layer even after 16 years.

5.2.2 Thermal insulation

In Figure 6, the effect of an artificial thermal insulation layer throughout the year is shown, presenting the monthly average evolution of the ground temperature profile of the Schilthorn borehole. We examine two cases with different thicknesses of the

thermal insulation layer of 50 mm and 100 mm. Although the placement of an insulation layer of 50 mm does not completely prevent temperatures above 0 °C (Figure 6a) it decreases the ALT in summer. In addition, Figures 6b and B1 demonstrate that the placement of an artificial insulation layer (Exp. #3, Table 3) effectively decreases the loss of heat to the atmosphere in winter. The distribution of heat flux in the permafrost remains preserved, due to the limitation in heat flux at the surface (Figure B1). However, in the long term, the combination of atmospheric and geothermal heat fluxes will warm the permafrost. Consequently, installation of an insulation layer of 50 mm thickness at the surface is insufficient to preserve the permafrost table, and the ALT still comprises several metres (Figure 6a, Table D1).
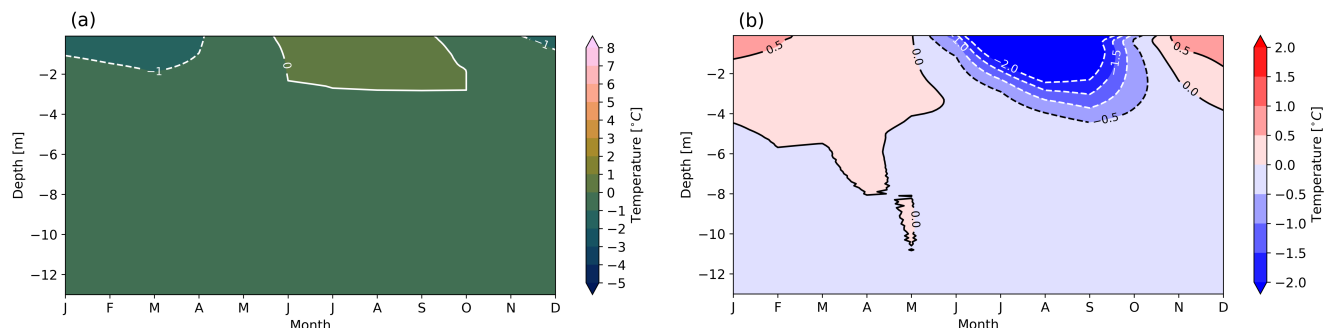
Figure 6. Modelled monthly averaged ground temperatures at the Schilthorn site for the period from 2000 to 2017 using a 50 mm artificial thermal insulation layer on top of the ground throughout the year (Exp. #3, Table 3). (a) Temperature evolution in the ground. (b) Temperature difference compared to the undisturbed natural conditions. Red (blue) colours indicate model temperature higher (lower) than measurements.

The results presented in Figure B2 show that the thicker the thermal insulation layer, the smaller its effect of thermal stabilisation. Instead of favouring ground cooling during winter, this artificial thermal insulation prevents the desired heat loss from the ground to the atmosphere. In addition, it can be seen that decreasing the thickness of the insulation layer allows some cooling in winter, but at the same time protects the ground less from heating in summer. The observed effects are plausible because snow accumulates above the thermal insulation layer in winter, reducing the loss of heat from the ground. This suggests the existence of an optimal thermal insulation thickness. However, this optimum naturally depends on latitude, altitude, exposition, slope angle, local topography, and climatic conditions. Given the principal interest in quantitatively assessing different engineering-based permafrost thermal stabilisation methods, we did not strive to determine this optimum for the Schilthorn site and consider it outside of the scope of this study. The brief conclusion here is that the 50 mm thickness yielded a better effect during summer and winter, compared to cases with increased (100 mm) and decreased (10 mm) layer thickness. However, it also appears that this method is not efficient enough to protect local alpine permafrost in the long term from the growing impact of atmospheric warming and increasing net energy input into the ground.
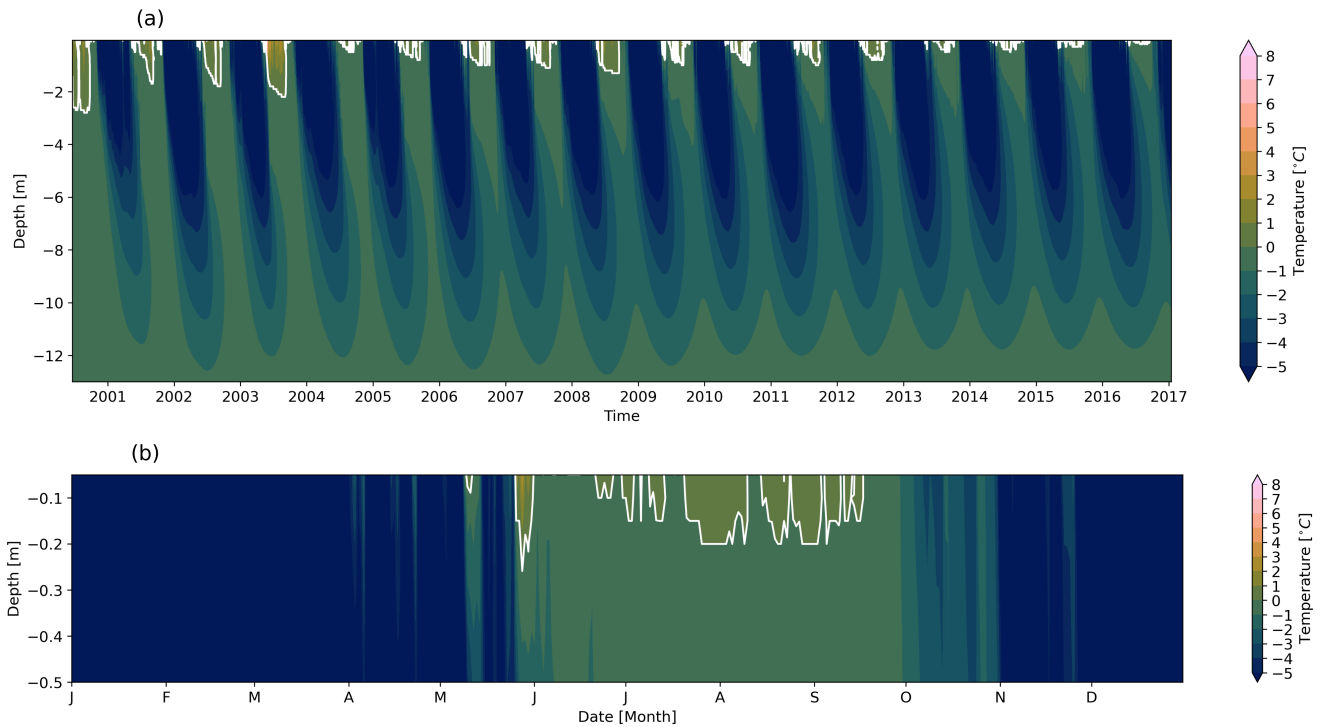
Figure 7. (a) Time series of daily averaged modelled ground temperatures from the heat transfer attenuation experiment, (Exp. #4, Table 3) at the Schilthorn site for the period of 2000 to 2017. White contours indicate the 0 °C isotherm, i.e., the ALT. (b) Last year of the simulation, 2016, after 16 years of artificial thermal insulation of the ground.

390   The timely placement/lifting of the insulation layer is the key to most effective cooling during winter and better preservation during summer. We examined the impact of heat transfer control by combining the impact of thermal insulation with surface shading. Figure 7 shows that this approach (Exp. #4, Table 3) results in intense winter cooling over a multi-year period while favouring heat loss from the ground to a depth of about 10 m (Figure 7a). In this case, heat flux attenuation (Sharaborova and Loktionov, 2022) is sufficient for thermal stabilisation of the permafrost (Table D1) and is more efficient in cooling when 395   installed on site than continuous thermal insulation (Luo et al., 2018). This method also results in a gradual decrease in ALT over the years, demonstrating that the winter cooling effect surpasses the summer warming. In addition, thermal insulation during the summer helps to protect the permafrost by reducing the transfer of heat from the atmosphere. Taking a closer look at the last year of the simulation (Figure 7b) reveals a temperature decrease in near-surface layers and a significant reduction in ALT with this approach. Figure B3 indicates the continuous loss of heat during winter, which explains the preservation of low 400   ground temperatures. This cooling mechanism can be sufficient for creating a thermal (cold) "barrier" layer near the surface to protect the ground underneath over a whole year (Figure 7). Although the creation of a "barrier" layer takes several years in the simulation, with unstable conditions occurring during its formation, after 16 years the ALT was decreased to several

decimetres. We expect this method to be even more effective when used in combination with active cooling since it creates an additional "shield" of thermal insulation and further decreases heat exchange with the atmosphere.

5.2.3 Thermal stabilisation with active cooling

We now examine the effect of the proposed thermal stabilisation system with active cooling (Section 4.2.3), first quantifying the effect of the cooling pipes alone (Exp. #5, Table 3) and then the combined effect of the system that includes shading of the ground from the solar panels (Exp. #6, Table 3). We examine the distribution of temperature and heat flux in the ground to observe whether a thermal barrier layer is developing.
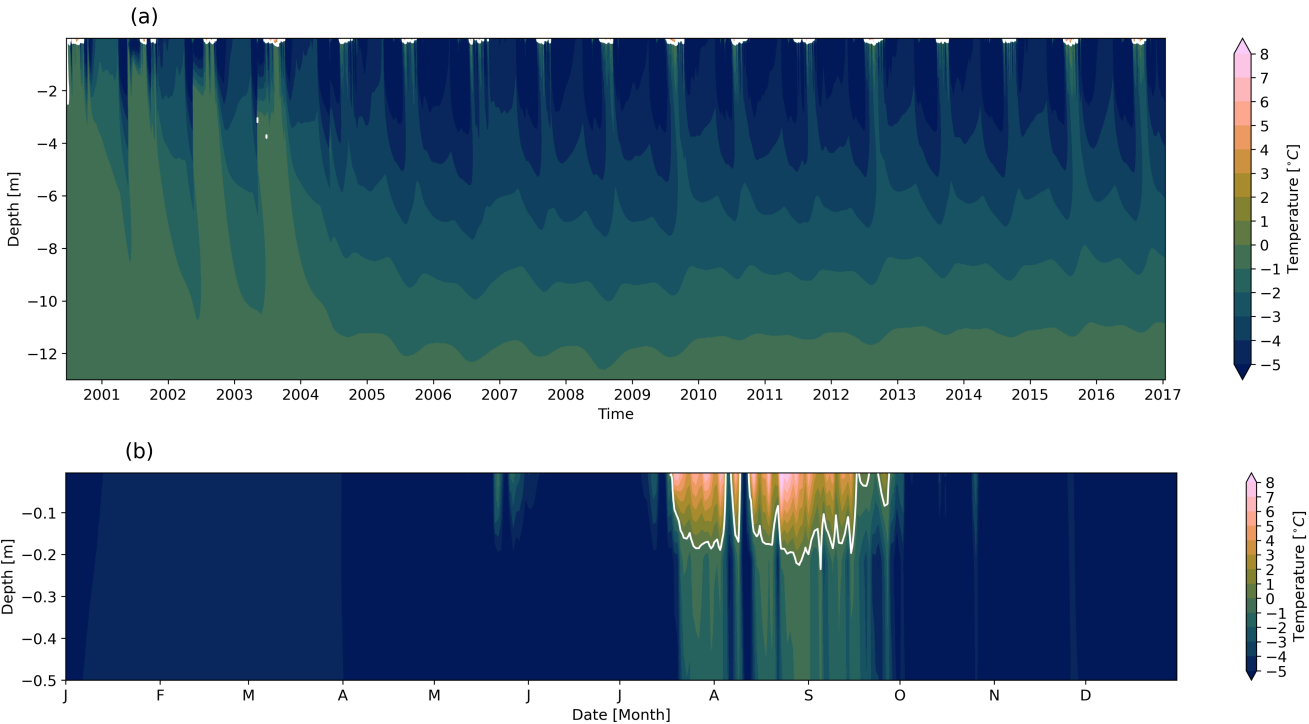
Figure 8. (a) Time series of daily averaged modelled ground temperatures from the cooling pipes experiment (Exp. #5, Table 3) at the Schilthorn site for the period of 2000 to 2017. White contours indicate the 0 °C isotherm, i.e., the ALT. (b) Last year of the simulation, 2016, after 16 years of active cooling.

Figure 8 shows that when active cooling is applied (Exp. #5, Table 3), sub-zero temperatures of the permafrost establish after 4 years with temperatures well below 0 °C at depth. The upper layers of the last simulated year (Figure 8b) show that the thawing boundary, indicated by the 0 °C contour, does not extend deeper than 25 cm demonstrating the effectiveness of the cooling method in creating a thermal barrier layer and limiting heat transfer during summer.

The distribution of heat flux shown in Figure 9 (Exp. #5, Table 3) illustrates the consequences of the formation of a thermal barrier layer. The large heat fluxes in the upper layers are due to the strong temperature gradient between the ground surface

and the cooling pipes, the latter conserving a constant low temperature around them. This determines the direction of the heat flux downward from the surface to the level of the pipes. In depth, the heat flux is directed upward toward the pipes. Together, these heat fluxes indicate the extraction of heat from the ground through the cooling liquid that circulates in the pipes.
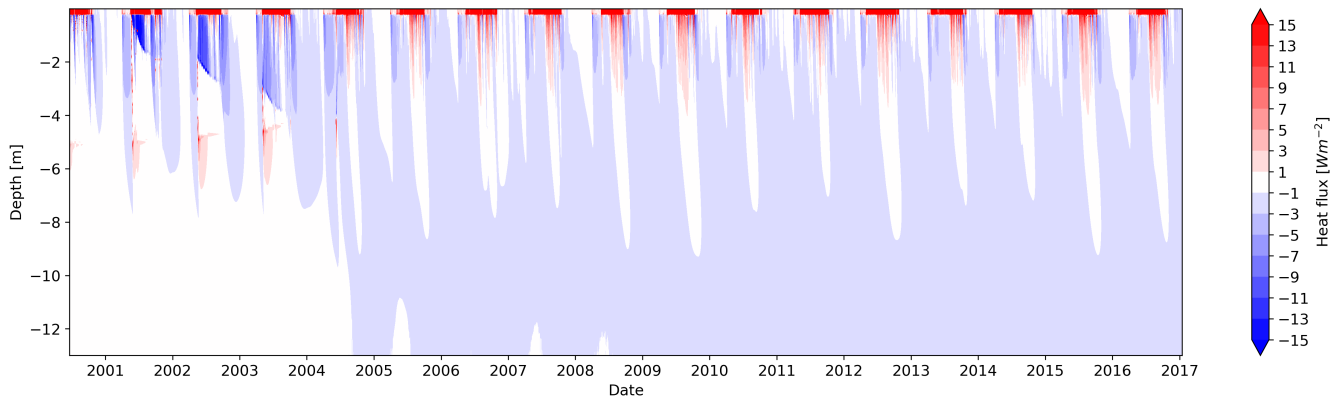
Figure 9. Time series of daily averaged modelled conductive heat flux from the cooling pipes experiment (Exp. #5, Table 3) at the Schilthorn site for the period of 2000 to 2017.

Figure 8a shows that after the establishment of the barrier layer (after about 4 years), the soil cools to a level of approximately 3 m, which may be related to the structural stratigraphy of the ground given (Table 2). Due to thermal inertia and slow heat conduction in the ground, it takes several years to form a stable thermal barrier layer (Figure 8). Once enough heat is lost from the ground, the system switches from cooling to keeping the in-depth temperatures stable in the following years. Due to the temperature boundary conditions at the bottom of the model domain (Section 4.1 the model evolves toward a steady state (Figure 9).

We now focus on the full system that combines active and passive cooling methods, i.e., including shading with the solar panels (Exp. #6, Table 3). The simulation results presented in Figure 10 show that this combined effect is favourable for the preservation of permafrost due to the formation of a more pronounced sub-freezing thermal barrier layer compared to the results of both systems independently. The effect is also more immediate and does not take several years to establish the thermal barrier layer (Figure 10a). In the last year of the simulation (Figure 10b), it is evident that the impact of summer warming cannot be fully suppressed or compensated for. However, the engineered cooling method significantly reduces the ALT compared to natural conditions, achieving a difference of several metres. Our results show that the combination of active and passive cooling is sufficient to stabilise not only the continuous permafrost of the lowlands, as shown by Loktionov et al. (2022), but also the mountain permafrost (Table D1).
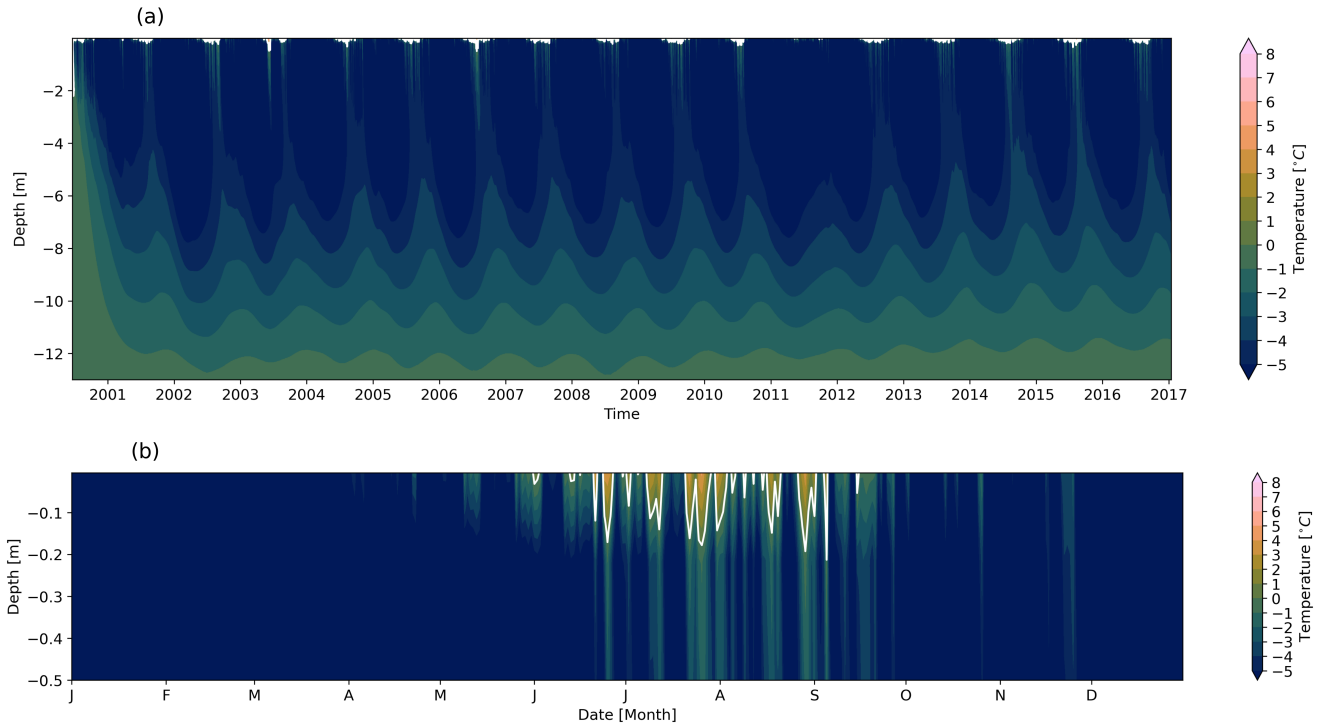
Figure 10. (a) Time series of daily averaged modelled ground temperatures from the experiment combining cooling pipes and solar panel shading (Exp. #6, Table 3) at the Schilthorn site for the period of 2000 to 2017. White contours indicate the 0 °C isotherm, i.e., the ALT. (b) Last year of the simulation, 2016, after 16 years of active cooling and shading.

The evolution of the conductive heat flux initiated by the combined cooling system (Exp. #6, Table 3)(Figure 11) shows
435   that in addition to the effect of the cooling pipes, passive cooling works during the winter season. This corresponds to the heat evacuation from the depth in winter, when the heat flux direction is upwards (Figure 11a). Figure 11b indicates that the highest heat flux values occur in the layer between the surface and the pipes from April to the end of October, when active cooling is applied. This downward heat flux extends to the cooling pipes, which arises as a result of the strongest temperature gradient. Below this level, the heat flux eventually decreases to $0 \ \mathrm{Wm^{-2}}$. In winter, heat is lost to the cold atmosphere, turning
440   the direction of heat conduction. Figure C1 presents the daily heat flux and temperature profiles, illustrating the evolution of conductive heat flux and ground temperatures over time and highlighting their dynamic behaviour throughout the simulation.
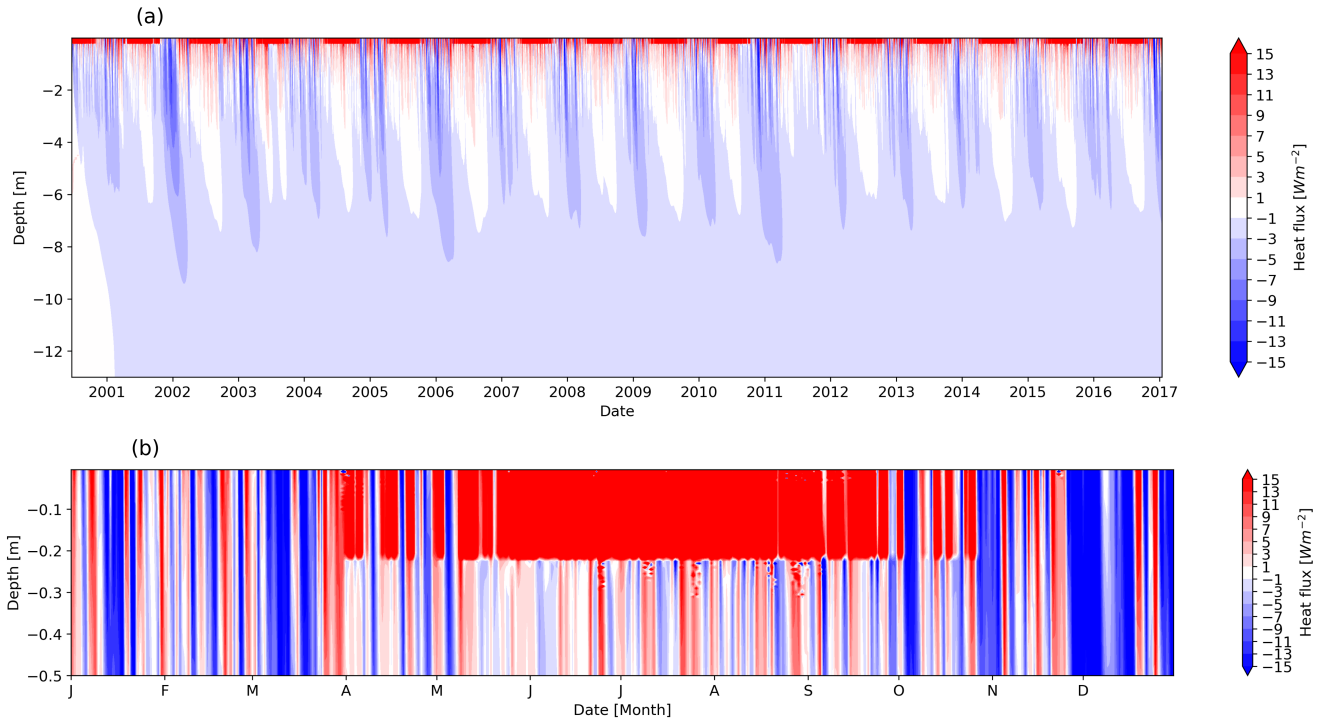
Figure 11. Time series of daily averaged modelled conductive heat flux from the experiment combining cooling pipes and solar panel shading (Exp. #6, Table 3) at the Schilthorn site for the period of 2000 to 2017. (b) Last year of the simulation, 2016, after 16 years of active cooling and shading.

5.3 Analysis and discussion of stabilisation effects

For the mountain regions considered, the most efficient method of thermal stabilisation was active cooling combined with effects from passive methods such as surface shading with solar panels. In the experiments described so far (Section 5.2.3) all the photovoltaic energy produced was used to power the heat pump. The main objective is to set as much energy as needed for cooling. However, we also tested the case where only a partial amount of the available PV energy is reserved for cooling. This case may serve as a more realistic and practical demonstration of the system application, as it could imply the potential to use smaller panels or other optimisations in system design. It allows for challenging the system, in case the surface for installation is limited and the energy should be redistributed between cooling and other infrastructure energy supply. We show a situation in which only 50% of the incident solar radiation is used to power the heat pump, i.e., for cooling (Exp. #7, Table 3), reserving the other half for the power grid or other needs in the vicinity of the site. Recall that the cooled surface has the same area as that of the solar panels (Section 4.2.3). In the following part, we perform some experimental tests, cutting the energy supply directed to cooling by a certain amount, to look at the resilience of the system in different configurations.

In the case where only half of the generated PV energy is used for cooling (Exp. #7, Figure 12), we applied cooling in summer, similarly to the case discussed in Section 5.2.3 Exp. #6, where cooling occurs from April to October. This energy

partition between cooling and the grid aims to maintain the same temperature and persistence of the barrier layer as in Exp. #6 (Figure 10). However, with half the amount of cooling power, the barrier layer is not as stable as with the 100% energy supply. In addition, the ALT increases when using less power (Figure 12b) compared to the case applying 100% (Figure 10b). Recall that the creation of an efficient barrier layer only with cooling pipes requires 5 full seasons with 100% power supply, applying cooling from April to October. It can be seen that, due to the initial adjustment process creating the thermal barrier layer, most of the PV energy is initially used to cool the system. Once the barrier layer is established and stable in time, a larger fraction of the produced PV energy can be injected into the grid. However, it is worth acknowledging that active cooling may not necessarily need to bring the system to a new equilibrium, and maintaining the existing thermal balance might be sufficient. It should be noted that our results did not explicitly test this; we assumed a simplified case in which the energy is evenly split between cooling and grid injection. In a real-world application, the system control will become completely dynamic, an ultimate goal of the system application. Priority should be given to cooling before feeding into the grid. For the design of a suitable PV system, it is therefore imperative to know the energy demand for the creation and maintenance of a thermal barrier layer in alpine permafrost, which can be obtained from numerical simulations, as demonstrated in the previous sections. The optimal choice will enable reliable cooling of the ground while bearing the potential of providing significant excess power to the grid or nearby installation, especially after the initial ramp-up time.
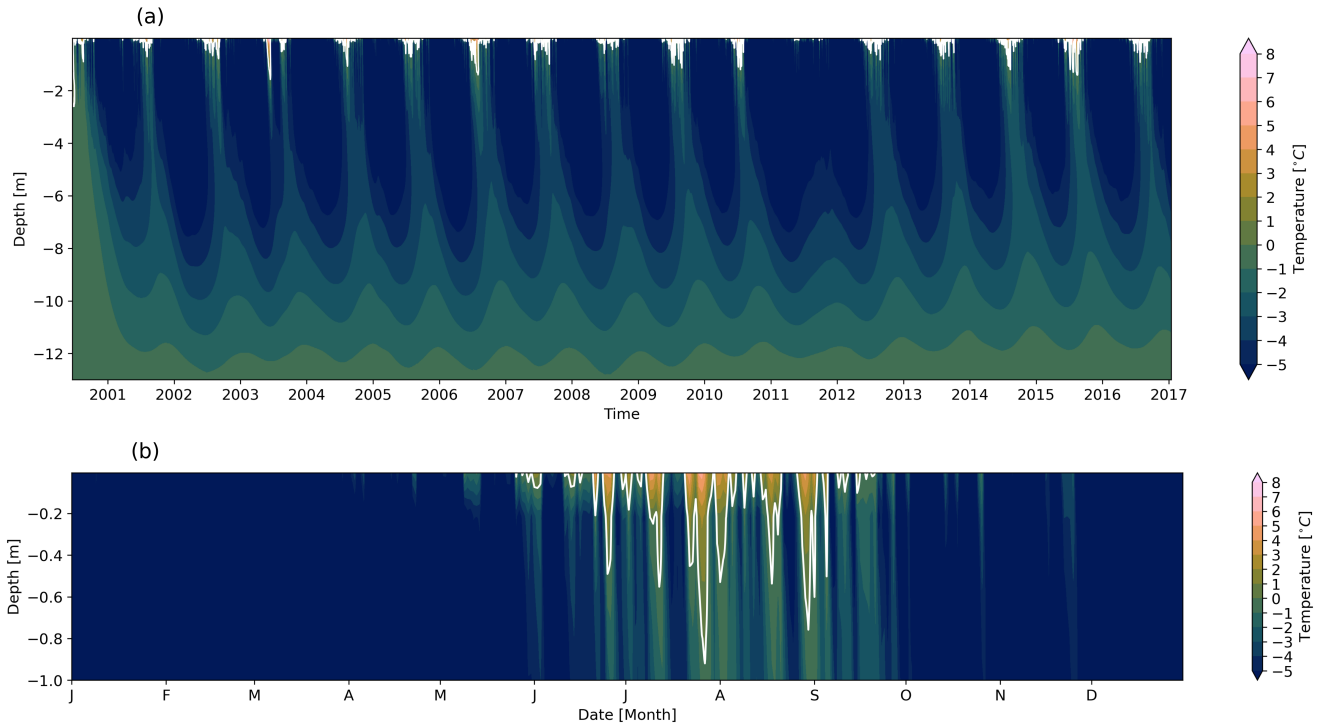
Figure 12. (a) Time series of daily averaged modelled ground temperatures from the experiment combining cooling pipes and solar panel shading but using only 50% of available energy for cooling (Exp. #7, Table 3) at the Schilthorn site for the period of 2000 to 2017. White contours indicate the 0 °C isotherm, i.e., the ALT. (b) Last year of the simulation, 2016, after 16 years of active cooling and shading.

Another alternative is the combination of active cooling (Exp. #6, Table 3) with heat flux attenuation (Exp. #4, Table 3) as discussed in Section 5.2.2 and presented in Figure 7, when during summer the ground was also protected with thermal insulation material. In that case, it is not necessary to wait until the snow has melted to lay out the thermal insulation as discussed in Section 5.2.2, however, it is important that the application of thermal insulation to attenuate heat flux is coordinated with the period of active cooling. During the active cooling period (April to October), thermal insulation is placed on the ground and removed when it is deactivated to allow effective winter cooling. This setup improves the efficiency of the cooling system by preserving low ground temperatures in summer while allowing natural cooling in winter. In this case, a 50 mm thick thermal insulation is simulated and was found to be efficient protection. The combination of active cooling, shading, and heat flux attenuation leads to the desired stabilisation effect. It allows us to use less PV energy for cooling and send more to the grid even in the case where the cooled surface area is equivalent to the surface of the solar panels used. As in experiments #7-#8, we tested different cases when only a certain amount of the available PV power is used for cooling. Here, due to the effective preservation of cold in the ground established by heat flux attenuation, we found for our test site that when combining active cooling with heat flux attenuation the energy required for cooling can be as low as 10% of the produced PV power (Exp. #8, Table 3).
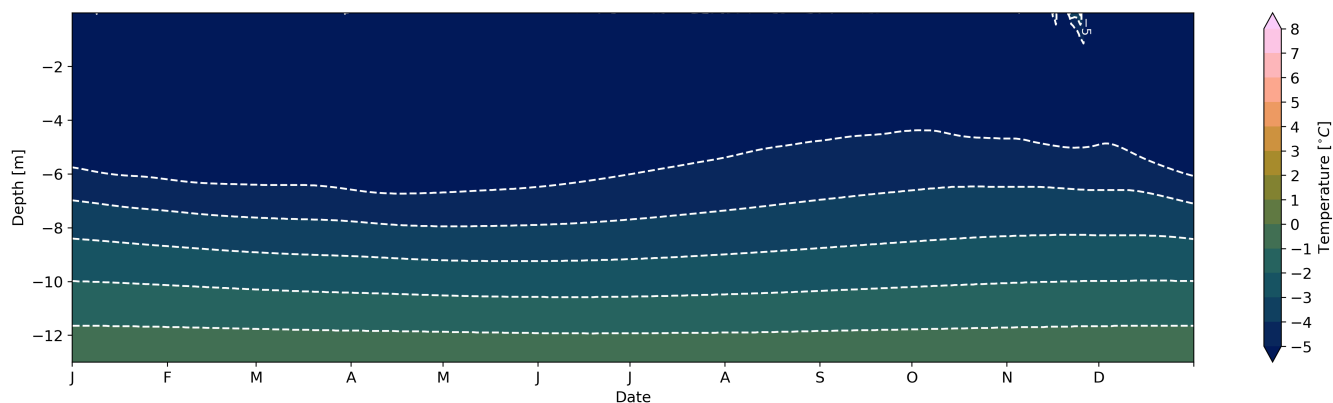
Figure 13. Daily averaged modelled temperature from the experiment combining heat flux attenuation by thermal insulation with active cooling and shading using only 10% of the produced PV power for cooling (Exp. #8, Table 3) at the Schilthorn showing the last year of the simulation, 2016, after 16 years of active and passive cooling.

As visible in Figure 13, the conservation of the cold temperature resulting from thermal insulation helps to keep the ALT shallow. This results in more efficient cooling and heat loss from the ground compared to cases of active cooling alone (Figure 8), or active cooling with shading (Figure 10). Another positive aspect of this combined method is that not all the PV power produced is used for cooling only, as was the case in Exp. #6 (Figure 10). Limiting the energy used for cooling without modifying the natural conductive heat flux is possible but recommended to be 50% or higher; otherwise, the active layer will remain deep. When combined with heat flux attenuation, this approach offers greater flexibility in managing the power received from solar panels. We also suggest that intense and continuous cooling might be unnecessary; it can be adjusted based on the monitored state of the permafrost, its temperatures, and also on atmospheric conditions. The latter determine which combinations of the stabilisation systems should be applied in different climatic conditions. Although site-specific decisions require local calibration, our simulations provide a basis for such adaptive strategies. The simulated ALT results are presented in Table D1 for a better overview and comparison.

Knowing the amount of energy required for cooling, creating and maintaining an effective thermal barrier layer to stabilise the underlying permafrost allows optimal system design and power regulation. Simulations have shown that only a fraction of the produced PV energy (50% for active cooling alone and 10% for active cooling combined with heat flux attenuation) is necessary for direct cooling of the ground. The excess energy is then available for the grid. In an advanced application, the stabilisation system could be dynamically regulated depending on the monitored state of the permafrost. However, optimal performance of the combination of active and passive cooling is difficult to achieve in the field due to local climate effects and complicated installation in complex alpine permafrost terrain. In such cases, the use of a system similar to Loktionov et al. (2024b) could be an alternative, cooling parts of constructions directly with cooling pipes attached to basement walls, taking advantage of unused space in the foundation of a building and avoiding the installation of cooling pipes on inaccessible surfaces such as bedrock.

Despite the efficiency of the cooling system and its ability to create a thermal barrier layer, additional aspects must be taken into account, for instance, the topography of the terrain, water in the ground and associated heave, and difficulties linked with building in mountain permafrost that may cause some risks to infrastructure and the cooling system itself. One of the dangers is moisture present in the substrate during active cooling (Section 5.2.3) which can lead to heave and potential destruction of cooling pipes and solar panels and cause damage to nearby structures. That is why for specific applications the simulated case must be adapted according to local ground properties and moisture conditions, the existing ground temperature distribution, ground-atmosphere heat exchange, topography, exposition, local climate, and potentially existing construction characteristics. It remains a challenge to apply a thermal stabilisation system in alpine permafrost without altering the structure and mechanical processes in the ground.

Up-scaling the system to larger cooling areas is another direction of research. The presented numerical modelling framework could be extended to other permafrost types, e.g. continuous (Arctic and Polar regions) and discontinuous (Subarctic regions), to investigate the performance of thermal stabilisation systems in different climatic regions and to propose an optimal combination of system components for these conditions. The present study constitutes a detailed and systematic numerical investigation of the choice and performance of permafrost stabilisation methods. The results are intended for the design and implementation of prototype installations and for up-scaling to real-world applications. The forthcoming challenges involve conducting experimental tests to validate the hypothesis, evaluating the influence of climate change on permafrost dynamics both with and without stabilisation measures, and devising an optimised methodology for thermal stabilisation tailored to diverse sites and climate conditions.

5.4 Model assumptions and limitations

In the following, we consider the limitations of the modelling framework and the implications of key assumptions that may influence the findings.

Due to the nature of simplified and idealised 1D simulations, that is, solar panels completely protect the ground without gaps between adjacent panels from snow and precipitation, no lateral snow drift, and the applied coefficient for wind speed decrease is empirical and its realistic value requires more advanced estimation (Sections 5.2.1 and 5.2). In addition, the use of one-dimensional simulations limits the investigation of three-dimensional effects such as subsurface lateral heat flow and complex geometric configurations of infrastructure. This simplification may not fully capture interactions present in real-world applications, particularly when optimising cooling pipe layouts under heterogeneous geo-cryologic conditions.

Another limitation of the 1D formulation is the representation of the pipe cooling system. The model prescribes a constant temperature in the pipe, not considering the fluid temperature difference at the entrance and exit of the pipe due to heat exchange with the surrounding ground, as would be the case in a 3D situation. Another approximation is that the calculation of the power required for cooling is simplified and is effective only in the presence of solar radiation. The current state of the model allows us to assess the thermal stabilisation potential of a system and show its effects when applied at a permafrost site. However, for a real-world application, a full 3D model and a real-time monitoring system should be used to dynamically adapt the necessary cooling power supply according to the conditions of the permafrost and the solar power production. In

540 addition, further refinement of the system is needed for an optimal choice of system variables such as the depth and spacing of the cooling pipes, the thickness of a thermal insulation layer, and the most efficient and economic way to create and maintain a thermal barrier layer while regulating power to dynamically adapt to real-time permafrost conditions and ALT. The geometric configuration of the cooling pipes in the ground needs to be adjusted to the local geo-cryologic, topographic, and climatic conditions for sufficient and most efficient ground cooling.

545 The simulation framework employs a bucket water scheme, which has inherent limitations in representing soil water retention and redistribution. Although more detailed approaches such as the Richards equation could capture capillary-driven and preferential flow, these rely on assumptions that may not hold in coarse, rocky permafrost soils where voids and cracks dominate and capillary action is minimal. Therefore, it is uncertain whether the Richards equation would offer improved accuracy in such terrain. Additionally, given the slope of the terrain at the site, percolating water may not only seep vertically 550 but also laterally, which is not accounted for in the current model. More relevant is probably considering slope flow and water percolation in a 3D version of the model.

Additionally, although SNOWPACK includes evaporation, its interaction with the bucket scheme simplifies the representation of latent heat exchange. In this model, only the surface layer contributes to evaporation, and once it dries out, evaporation ceases. This limits the model's ability to simulate continuous moisture-driven cooling via latent heat fluxes.

555 **6 Conclusions**

Thawing permafrost triggers hazards such as structural damage, rockfalls, and landslides, which increasingly threaten the stability of mountain infrastructure, while current mitigation methods struggle to adapt to rapid climate change. This study investigates the Schilthorn site in the Bernese Alps, Switzerland, where the ALT has doubled over the past decade, highlighting its vulnerability to climate change. Using the 1D SNOWPACK model, validated with borehole temperature data, we simulate 560 and assess various passive and active thermal stabilisation strategies (Table 3). These methods aim to cool the ground, regulate seasonal heat exchange, and reduce ALT. One approach establishes a cold thermal barrier powered by collocated solar panels that also shade the surface. After simulating natural site conditions, we test multiple stabilisation systems. Results show that while all methods reduce ground temperatures, combined systems are most effective, with performance depending on the strategy applied.

565 The simulation results of passive thermal stabilisation with shading of the surface (Section 4.2.1) indicated that this measure alone is not sufficient to create long-term thermal stabilisation of permafrost. It has a good effect during winter, due to natural cooling; in summer, however, the ALT stays almost unchanged compared to natural conditions (Section 5.2.1). Another passive cooling system consists of a thermal insulation layer on top of the ground (Section 4.2.2). Covering the ground year-round with insulation material does not result in significant thermal stabilisation, while deploying and lifting the insulation layer depending 570 on the season effectively regulate the conductive heat flux near the ground surface, leading to favourable stabilisation effects (Section 5.2.2). The thermal stabilisation seasonal heat flux attenuation method significantly reduces the ALT, although it takes several years to fully achieve this effect.

A pipe system in the ground for active cooling (Section 4.2.3) can create a stable continuous thermal barrier layer but only after a period of 4 years (Section 5.2.3). The best efficiency of a thermal stabilisation system is achieved by combining active and passive methods (Section 5.2.3), which decreases the ALT to only a few tens of centimetres, and results in a stable barrier layer already after the first year simulated. The combination of active cooling, shading, and heat flux attenuation with a temporary thermal insulation layer that reduces warming in summer and favours cooling in winter has the strongest effect (Section 5.3).

We showed the ability of thermal stabilisation methods using renewable energy to delay thawing, protecting exposed infrastructure with adaptable and scalable cooling techniques. This study demonstrates that thermal stabilisation methods applied in alpine permafrost work as effectively as they do in lowland permafrost. Given their comparable success in different soil types, these methods can be broadly applied to alpine permafrost, extending beyond the specific site studied.

Code and data availability. Data for running the simulations as well as the output results are accessible via https://www.doi.org/10.16904/envidat.678. The SNOWPACK model is available at http://models.slf.ch. The version used in this study corresponds to /branches/limiting_adv_heat.

 Appendix A: Natural conditions
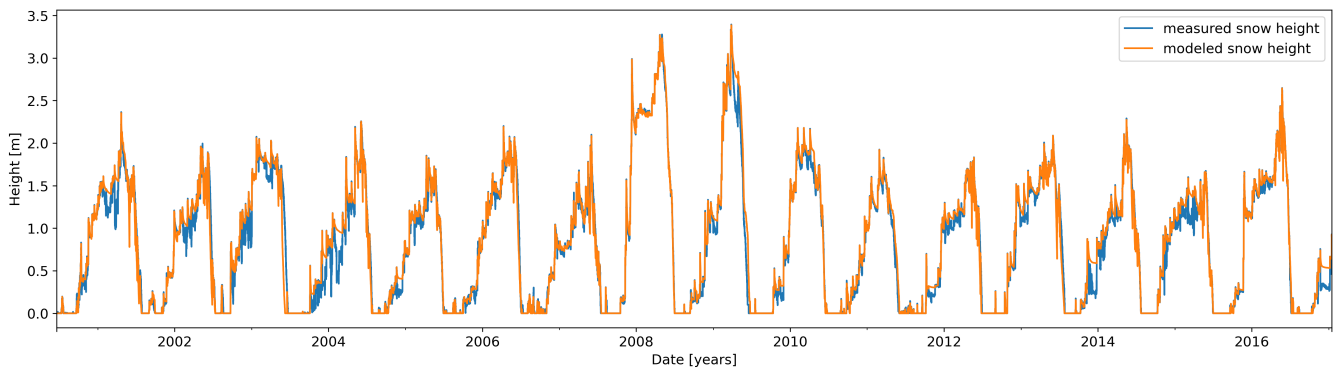
A1   Snow height

Figure A1. Time series of daily averaged measured and modelled snow height during natural undisturbed conditions at the Schilthorn site from 2000 to 2017.

A2   Ground temperatures
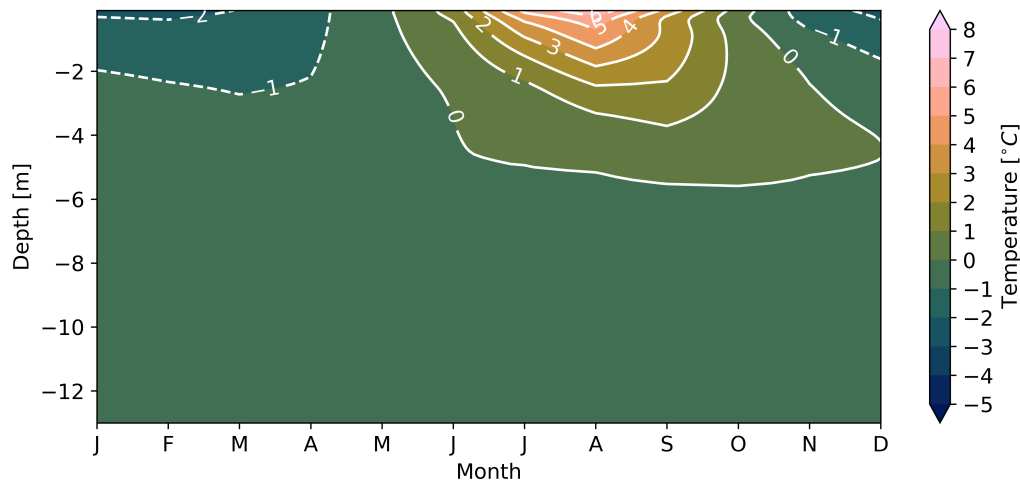
Figure A2. Monthly averaged modelled ground temperatures resulting from natural undisturbed conditions at the Schilthorn site from 2000 to 2017.

Appendix B: Thermal stabilisation with thermal insulation

B1 Thermal insulation conductive heat flux distribution
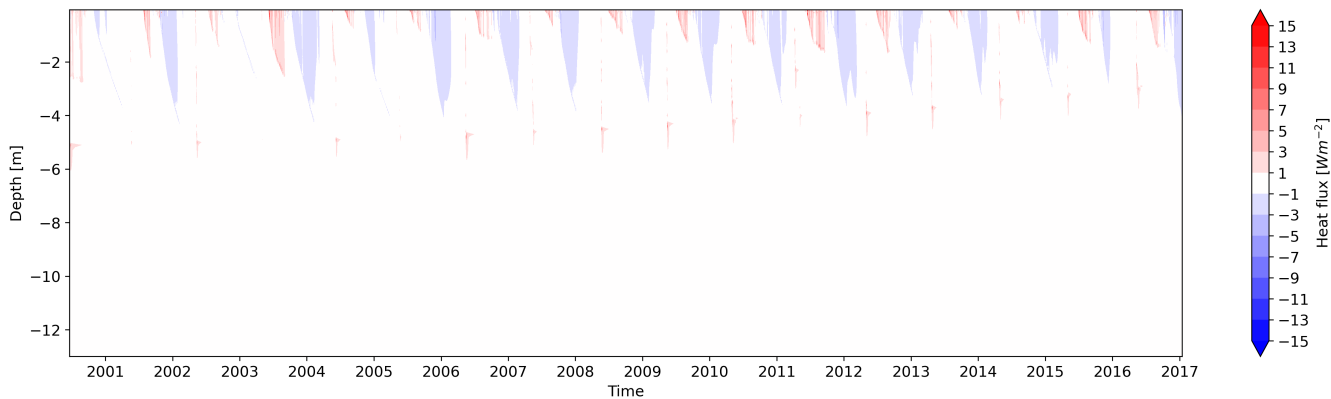
Figure B1. Time series of daily averaged modelled conductive heat flux from thermal insulation experiment using 50 mm thermal insulation layer at the Schilthorn site for the period of 2000 to 2017.

590 ### B2 Thermal insulation thickness effect
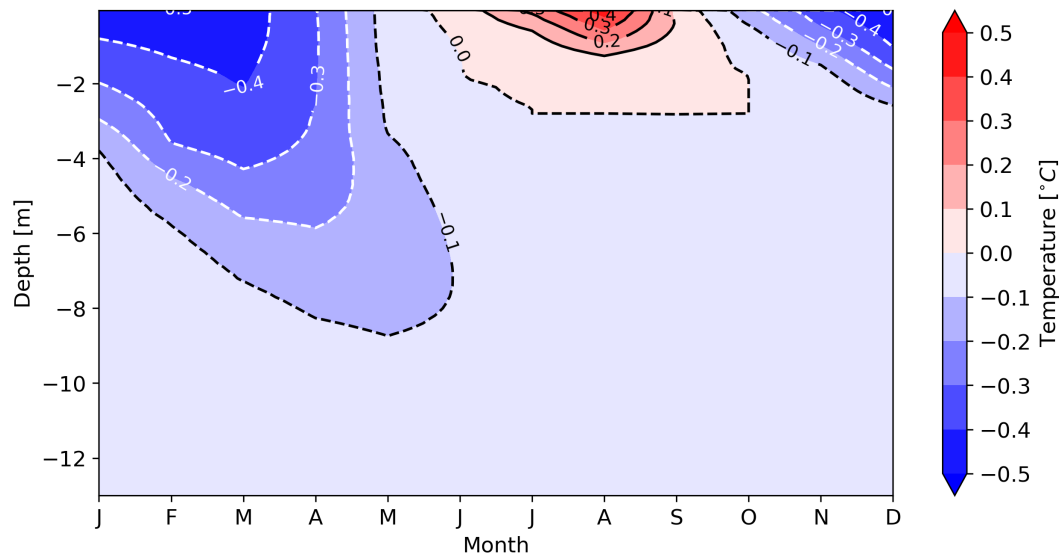
Figure B2. Monthly averaged temperature differences between 50 mm and 100 mm thermal insulation thicknesses.

B3   Heat flux attenuation distribution of conductive heat fluxes
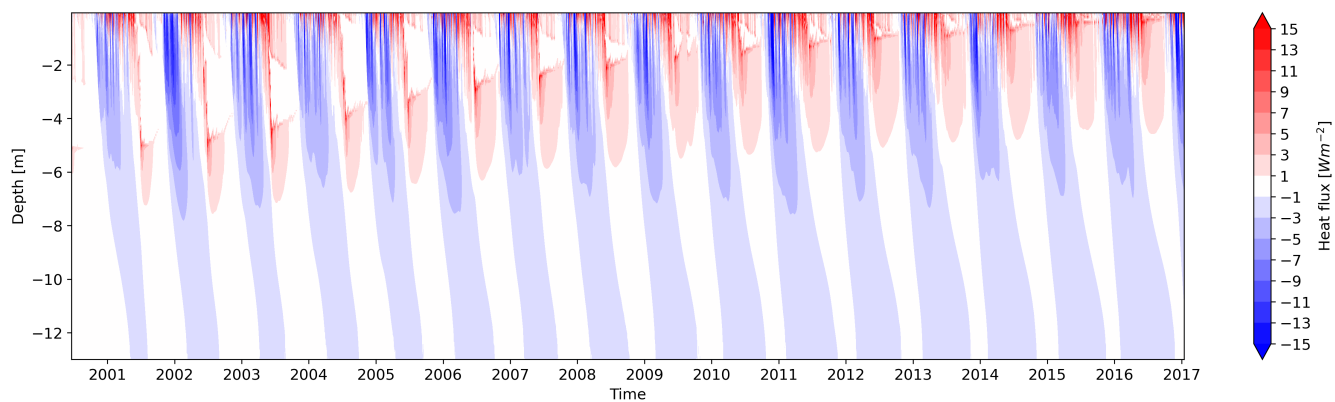
Figure B3. Time series of daily averaged modelled conductive heat flux from the heat transfer attenuation experiment at the Schilthorn site for the period of 2000 to 2017.

Appendix C: Thermal stabilisation with active cooling
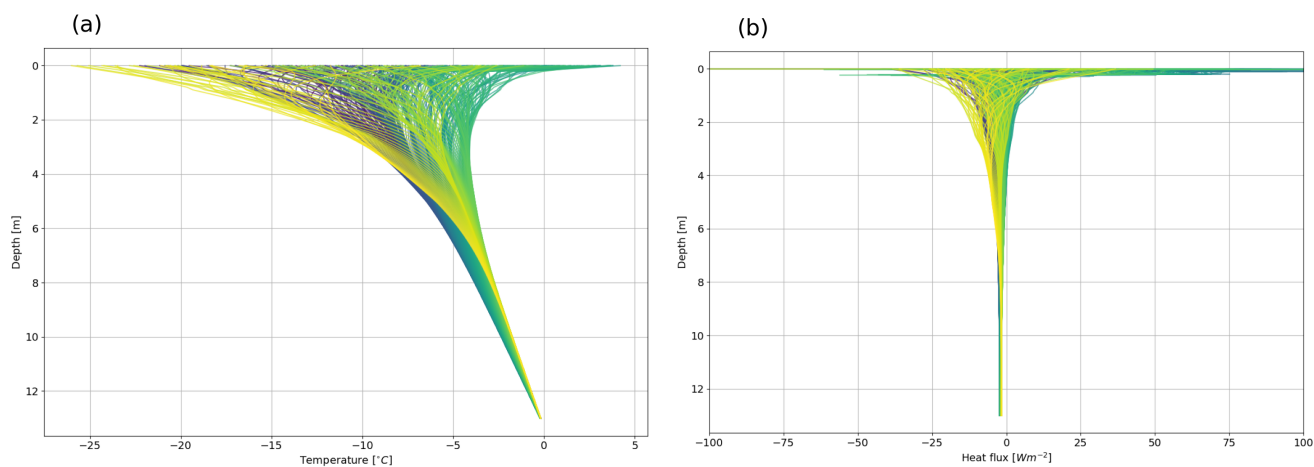
Figure C1. (a) Daily averaged temperature distribution, and (b) daily averaged heat flux distribution for the last year of the simulations, 2016 after 16 years of active cooling and shading.

Appendix D: Thermal stabilisation methods comparison

Table D1. Thermal stabilisation methods comparison.

Experiment number	Model simulation	Max ALT after 16 years, m	Max of monthly averaged ALT over 16 years, m
1	Natural conditions	6.20	5.59
2	Shading of the surface	3.40	2.77
3	Thermal insulation (50 mm) all year round	1.50	2.80
4	Heat flux attenuation	0.26	1.01
5	Active cooling (cooling pipes alone)	0.23	0.12
6	Active and passive cooling (cooling pipes and solar panels)	0.21	0
7	Active and passive cooling (cooling pipes and solar panels) using 50% of energy for cooling	0.92	0.07
8	Active and passive cooling (cooling pipes and solar panels) using 10% of energy for cooling combined with heat flux attenuation	0	0

Author contributions. ES, ML and HH designed the research. ES prepared the data, run the simulations, analysed results and wrote the draft. ML, NW, MP, HH contributed to the results and data analysis and revised the manuscript. ML and HH supervised the research. NW maintained and corrected the SNOWPACK code. MP provided expertise in permafrost processes. All authors contributed to the final version of the manuscript.

Competing interests. The corresponding author has declared that none of the authors have any known competing financial interests or personal relationships that could have influenced the work reported in this paper.

Acknowledgements. We acknowledge MeteoSwiss, IMIS, and PERMOS for providing the observational data used in this research. We are grateful to Prof. Hanna Lee, the editor, for her valuable feedback and insightful comments, which greatly improved this manuscript. We appreciate team at the Department of Geosciences, University of Fribourg, for their helpful feedback. We thank Dr. Sergi Gonzàlez Herrero for his suggestions on data presentation and analysis, as well as his valuable recommendations. We acknowledge Egor Yu. Loktionov for his contribution to the development and patenting of the thermal stabilization method employed in this work. We acknowledge the

605   funding support of Swiss Government Excellence Scholarship #2022.0064. Finally, we acknowledge the two anonymous reviewers for their constructive comments and suggestions that enhanced the quality of the manuscript.

References

Alekseev, A., Gribovskii, G., and Vinogradova, S.: Comparison of analytical solution of the semi-infinite problem of soil freezing with numerical solutions in various simulation software, IOP Conference Series: Materials Science and Engineering, 365, 042059, https://doi.org/10.1088/1757-899X/365/4/042059, 2018.

Asanov, I. M. and Loktionov, E. Y.: Possible benefits from PV modules integration in railroad linear structures, Renewable Energy Focus, 25, 1–3, https://doi.org/10.1016/j.ref.2018.02.003, 2018.

Bavay, M. and Egger, T.: MeteoIO 2.4.2: a preprocessing library for meteorological data, Geoscientific Model Development, 7, 3135–3151, https://doi.org/10.5194/gmd-7-3135-2014, 2014.

Biskaborn, B. K., Smith, S. L., Noetzli, J., Matthes, H., Vieira, G., Streletskiy, D. A., Schoeneich, P., Romanovsky, V. E., Lewkowicz, A. G., Abramov, A., Allard, M., Boike, J., Cable, W. L., Christiansen, H. H., Delaloye, R., Diekmann, B., Drozdov, D., Etzelmüller, B., Grosse, G., Guglielmin, M., Ingeman-Nielsen, T., Isaksen, K., Ishikawa, M., Johansson, M., Johannsson, H., Joo, A., Kaverin, D., Kholodov, A., Konstantinov, P., Kröger, T., Lambiel, C., Lanckman, J.-P., Luo, D., Malkova, G., Meiklejohn, I., Moskalenko, N., Oliva, M., Phillips, M., Ramos, M., Sannel, A. B. K., Sergeev, D., Seybold, C., Skryabin, P., Vasiliev, A., Wu, Q., Yoshikawa, K., Zheleznyak, M., and Lantuit, H.: Permafrost is warming at a global scale, Nature Communications, 10, 264, https://doi.org/10.1038/s41467-018-08240-4, number: 1 Publisher: Nature Publishing Group, 2019.

Bommer, C., Phillips, M., and Arenson, L. U.: Practical recommendations for planning, constructing and maintaining infrastructure in mountain permafrost, Permafrost and Periglacial Processes, 21, 97–104, https://doi.org/10.1002/ppp.679, _eprint: https://onlinelibrary.wiley.com/doi/pdf/10.1002/ppp.679, 2010.

Chen, Y., Mandal, J., Li, W., Smith-Washington, A., Tsai, C.-C., Huang, W., Shrestha, S., Yu, N., Han, R. P. S., Cao, A., and Yang, Y.: Colored and paintable bilayer coatings with high solar-infrared reflectance for efficient cooling, Science Advances, 6, eaaz5413, https://doi.org/10.1126/sciadv.aaz5413, publisher: American Association for the Advancement of Science, 2020.

Cheng, G.: A roadbed cooling approach for the construction of Qinghai–Tibet Railway, Cold Regions Science and Technology, 42, 169–176, https://doi.org/10.1016/j.coldregions.2005.01.002, 2005.

Duvillard, P. A., Ravanel, L., Schoeneich, P., Deline, P., Marcer, M., and Magnin, F.: Qualitative risk assessment and strategies for infrastructure on permafrost in the French Alps, Cold Regions Science and Technology, 189, 103311, https://doi.org/10.1016/j.coldregions.2021.103311, 2021.

Ekici, A., Chadburn, S., Chaudhary, N., Hajdu, L. H., Marmy, A., Peng, S., Boike, J., Burke, E., Friend, A. D., Hauck, C., Krinner, G., Langer, M., Miller, P. A., and Beer, C.: Site-level model intercomparison of high latitude and high altitude soil thermal dynamics in tundra and barren landscapes, The Cryosphere, 9, 1343–1361, https://doi.org/10.5194/tc-9-1343-2015, publisher: Copernicus GmbH, 2015.

Etzelmüller, B., Guglielmin, M., Hauck, C., Hilbich, C., Hoelzle, M., Isaksen, K., Noetzli, J., Oliva, M., and Ramos, M.: Twenty years of European mountain permafrost dynamics—the PACE legacy, Environmental Research Letters, 15, 104070, https://doi.org/10.1088/1748-9326/abae9d, publisher: IOP Publishing, 2020.

Farinotti, D., Usselmann, S., Huss, M., Bauder, A., and Funk, M.: Runoff evolution in the Swiss Alps: projections for selected high-alpine catchments based on ENSEMBLES scenarios, Hydrological Processes, 26, 1909–1924, https://doi.org/10.1002/hyp.8276, publisher: John Wiley & Sons, Ltd, 2012.

Grünewald, T., Wolfsperger, F., and Lehning, M.: Snow farming: conserving snow over the summer season, The Cryosphere, 12, 385–400, https://doi.org/10.5194/tc-12-385-2018, 2018.

Haberkorn, A., Wever, N., Hoelzle, M., Phillips, M., Kenner, R., Bavay, M., and Lehning, M.: Distributed snow and rock temperature modelling in steep rock walls using Alpine3D, The Cryosphere, 11, 585–607, https://doi.org/10.5194/tc-11-585-2017, 2017.

Haeberli, W. and Gruber, S.: Global Warming and Mountain Permafrost, pp. 205–218, Springer Berlin Heidelberg, Berlin, Heidelberg, ISBN 978-3-540-69371-0, https://doi.org/10.1007/978-3-540-69371-0_14, 2009.

Haeberli, W., Noetzli, J., Arenson, L., Delaloye, R., Gärtner-Roer, I., Gruber, S., Isaksen, K., Kneisel, C., Krautblatter, M., and Phillips, M.: Mountain permafrost: development and challenges of a young research field, Journal of Glaciology, 56, 1043–1058, https://doi.org/10.3189/002214311796406121, 2010.

Haeberli, W., Schaub, Y., and Huggel, C.: Increasing risks related to landslides from degrading permafrost into new lakes in deglaciating mountain ranges, Geomorphology, 293, 405–417, https://doi.org/https://doi.org/10.1016/j.geomorph.2016.02.009, permafrost and periglacial research from coasts to mountains, 2017.

Haeberli, W., Noetzli, J., and Mühll, D. V.: Using Borehole Temperatures for Knowledge Transfer about Mountain Permafrost: The Example of the 35-year Time Series at Murtèl-Corvatsch (Swiss Alps), Journal of Alpine Research | Revue de géographie alpine, https://doi.org/10.4000/rga.11950, number: 111-2 Publisher: Association pour la diffusion de la recherche alpine et UGA Éditions., 2023.

Harris, C., Arenson, L. U., Christiansen, H. H., Etzelmüller, B., Frauenfelder, R., Gruber, S., Haeberli, W., Hauck, C., Hölzle, M., Humlum, O., Isaksen, K., Kääb, A., Kern-Lütschg, M. A., Lehning, M., Matsuoka, N., Murton, J. B., Nötzli, J., Phillips, M., Ross, N., Seppälä, M., Springman, S. M., and Vonder Mühll, D.: Permafrost and climate in Europe: Monitoring and modelling thermal, geomorphological and geotechnical responses, Earth-Science Reviews, 92, 117–171, https://doi.org/https://doi.org/10.1016/j.earscirev.2008.12.002, 2009a.

Harris, C., Arenson, L. U., Christiansen, H. H., Etzelmüller, B., Frauenfelder, R., Gruber, S., Haeberli, W., Hauck, C., Hölzle, M., Humlum, O., Isaksen, K., Kääb, A., Kern-Lütschg, M. A., Lehning, M., Matsuoka, N., Murton, J. B., Nötzli, J., Phillips, M., Ross, N., Seppälä, M., Springman, S. M., and Vonder Mühll, D.: Permafrost and climate in Europe: Monitoring and modelling thermal, geomorphological and geotechnical responses, Earth-Science Reviews, 92, 117–171, https://doi.org/10.1016/j.earscirev.2008.12.002, 2009b.

Hauck, C.: Frozen ground monitoring using DC resistivity tomography, Geophysical Research Letters, 29, 12–1–12–4, https://doi.org/10.1029/2002GL014995, _eprint: https://onlinelibrary.wiley.com/doi/pdf/10.1029/2002GL014995, 2002.

Hauck, C. and Hilbich, C.: Preconditioning of mountain permafrost towards degradation detected by electrical resistivity, Environmental Research Letters, 19, 064 010, https://doi.org/10.1088/1748-9326/ad3c55, publisher: IOP Publishing, 2024.

Hilbich, C.: Time-lapse refraction seismic tomography for the detection of ground ice degradation, The Cryosphere, 4, 243–259, https://doi.org/10.5194/tc-4-243-2010, publisher: Copernicus GmbH, 2010.

Hjort, J., Karjalainen, O., Aalto, J., Westermann, S., Romanovsky, V. E., Nelson, F. E., Etzelmüller, B., and Luoto, M.: Degrading permafrost puts Arctic infrastructure at risk by mid-century, Nature Communications, 9, 5147, https://doi.org/10.1038/s41467-018-07557-4, number: 1 Publisher: Nature Publishing Group, 2018.

Hjort, J., Streletskiy, D., Doré, G., Wu, Q., Bjella, K., and Luoto, M.: Impacts of permafrost degradation on infrastructure, Nature Reviews Earth & Environment, 3, 24–38, https://doi.org/10.1038/s43017-021-00247-8, 2022.

Hoelzle, M., Hauck, C., Mathys, T., Noetzli, J., Pellet, C., and Scherler, M.: Long-term energy balance measurements at three different mountain permafrost sites in the Swiss Alps, Earth System Science Data, 14, 1531–1547, https://doi.org/10.5194/essd-14-1531-2022, publisher: Copernicus GmbH, 2022.

Holtslag, A. a. M. and Bruin, H. A. R. D.: Applied Modeling of the Nighttime Surface Energy Balance over Land, Journal of Applied Meteorology and Climatology, 27, 689–704, https://doi.org/10.1175/1520-0450(1988)027<0689:AMOTNS>2.0.CO;2, publisher: American Meteorological Society Section: Journal of Applied Meteorology and Climatology, 1988.

Hu, T.-f., Liu, J.-k., Hao, Z.-h., and Chang, J.: Design and experimental study of a solar compression refrigeration apparatus (SCRA) for embankment engineering in permafrost regions, Transportation Geotechnics, 22, 100 311, https://doi.org/10.1016/j.trgeo.2019.100311, 2020.

685 Huss, M., Farinotti, D., Bauder, A., and Funk, M.: Modelling runoff from highly glacierized alpine drainage basins in a changing climate, Hydrological Processes, 22, 3888–3902, https://doi.org/10.1002/hyp.7055, _eprint: https://onlinelibrary.wiley.com/doi/pdf/10.1002/hyp.7055, 2008.

Instanes, A. and Mjureke, D.: Svalbard airport runway. Performance during a climate-warming scenario., Proceedings of the international conferences on the bearing capacity of roads, railways and airfields, https://www.ntnu.no/ojs/index.php/BCRRA/article/view/3224, 2005.

690 Jansson, P.-E. and Karlberg, L.: Coupled heat and mass transfer model for soil-plant-atmosphere systems. Royal Institute of Technology, Department of Civil and Environmental Engineering, Stockholm, 2004.

Kenner, R.: Permafrost distribution in Switzerland: Ground temperatures and ice content (2018), Zenodo, https://doi.org/10.5281/zenodo.1470165, 2018.

Kenner, R., Noetzli, J., Hoelzle, M., Raetzo, H., and Phillips, M.: Distinguishing ice-rich and ice-poor permafrost to map ground temperatures
695 and ground ice occurrence in the Swiss Alps, The Cryosphere, 13, 1925–1941, https://doi.org/10.5194/tc-13-1925-2019, 2019.

Kenner, R., Noetzli, J., Bazargan, M., and Scherrer, S. C.: Response of alpine ground temperatures to a rising atmospheric 0 °C isotherm in the period 1955–2021, Science of The Total Environment, 924, 171 446, https://doi.org/10.1016/j.scitotenv.2024.171446, 2024.

Lehning, M., Bartelt, P., Brown, B., Russi, T., Stöckli, U., and Zimmerli, M.: snowpack model calculations for avalanche warning based upon a new network of weather and snow stations, Cold Regions Science and Technology, 30, 145–157,
700 https://doi.org/https://doi.org/10.1016/S0165-232X(99)00022-1, 1999a.

Lehning, M., Bartelt, P., Brown, B., Russi, T., Stöckli, U., and Zimmerli, M.: snowpack model calculations for avalanche warning based upon a new network of weather and snow stations, Cold Regions Science and Technology, 30, 145–157, https://doi.org/10.1016/S0165-232X(99)00022-1, 1999b.

Lehning, M., Doorschot, J., and Bartelt, P.: A snowdrift index based on SNOWPACK model calculations, Annals of Glaciology, 31, 382–386,
705 https://doi.org/10.3189/172756400781819770, 2000.

Lehning, M., Bartelt, P., Brown, B., Fierz, C., and Satyawali, P.: A physical SNOWPACK model for the Swiss avalanche warning: Part II. Snow microstructure, Cold Regions Science and Technology, 35, 147–167, https://doi.org/10.1016/S0165-232X(02)00073-3, 2002.

Li, F., Qin, Y., Wu, B., and Wang, T.: Experimental study on the cooling performance of shading boards with different emissivities at the underside, Cold Regions Science and Technology, 169, 102 902, https://doi.org/10.1016/j.coldregions.2019.102902, 2020.

710 Liu, B. Y. H. and Jordan, R. C.: The interrelationship and characteristic distribution of direct, diffuse and total solar radiation, Solar Energy, 4, 1–19, https://doi.org/10.1016/0038-092X(60)90062-1, 1960.

Loktionov, E., Klokov, A., Tutunin, A., Bakhmadov, A., Sharaborova, E., Sepitko, T., Churkin, S., and Korshunov, A.: Permafrost thermal stabilization using renewable energy sources, Tech. rep., International Permafrost Association (IPA), https://doi.org/10.52381/ICOP2024.152.1, 2024a.

715 Loktionov, E. Y., Sharaborova, E. S., and Asanov, I. M.: Prospective Sites for Solar-Powered Permafrost Stabilization Systems Integration in Russian Railways, in: 2019 8th International Conference on Renewable Energy Research and Applications (ICRERA), pp. 568–572, https://doi.org/10.1109/ICRERA47325.2019.8996544, iSSN: 2572-6013, 2019.

Loktionov, E. Y., Sharaborova, E. S., and Shepitko, T. V.: A sustainable concept for permafrost thermal stabilization, Sustainable Energy Technologies and Assessments, 52, 102 003, https://doi.org/10.1016/j.seta.2022.102003, 2022.

720 Loktionov, E. Y., Sharaborova, E. S., Klokov, A. V., Maslakov, A. A., Sotnikova, K. S., and Korshunov, A. A.: Ice cellars preservation technologies to ensure sustainable development of northern settlements, Arctic: Ecology and Economy, 14, 116–126, https://doi.org/10.25283/2223-4594-2024-1-116-126, (In Russian), 2024b.

Luethi, R., Phillips, M., and Lehning, M.: Estimating Non-Conductive Heat Flow Leading to Intra-Permafrost Talik Formation at the Riti-graben Rock Glacier (Western Swiss Alps), Permafrost and Periglacial Processes, 28, 183–194, https://doi.org/10.1002/ppp.1911, _eprint:
725 https://onlinelibrary.wiley.com/doi/pdf/10.1002/ppp.1911, 2017.

Luetschg, M., Lehning, M., and Haeberli, W.: A sensitivity study of factors influencing warm/thin permafrost in the Swiss Alps, Journal of Glaciology, 54, 696–704, https://doi.org/10.3189/002214308786570881, 2008.

Luo, J., Niu, F., Liu, M., Lin, Z., and Yin, G.: Field experimental study on long-term cooling and deformation charac-teristics of crushed-rock revetment embankment at the Qinghai–Tibet Railway, Applied Thermal Engineering, 139, 256–263,
730 https://doi.org/10.1016/j.applthermaleng.2018.04.138, 2018.

Lütschg, M.: A Model and Field Analysis of the Interaction Between Snow Cover and Alpine Permafrost, Physische Geographie, Geographis-ches Institut der Universität Zürich, ISBN 9783855432431, https://books.google.ch/books?id=-_37NAAACAAJ, 2005.

Marmy, A., Salzmann, N., Scherler, M., and Hauck, C.: Permafrost model sensitivity to seasonal climatic changes and extreme events in mountainous regions, Environmental Research Letters, 8, 035 048, https://doi.org/10.1088/1748-9326/8/3/035048, publisher: IOP Pub-
735 lishing, 2013.

Marmy, A., Rajczak, J., Delaloye, R., Hilbich, C., Hoelzle, M., Kotlarski, S., Lambiel, C., Noetzli, J., Phillips, M., Salzmann, N., Staub, B., and Hauck, C.: Semi-automated calibration method for modelling of mountain permafrost evolution in Switzerland, The Cryosphere, 10, 2693–2719, https://doi.org/10.5194/tc-10-2693-2016, 2016.

Mergili, M., Jaboyedoff, M., Pullarello, J., and Pudasaini, S. P.: Back calculation of the 2017 Piz Cengalo–Bondo landslide cascade with
740 r.avaflow: what we can do and what we can learn, Natural Hazards and Earth System Sciences, 20, 505–520, https://doi.org/10.5194/nhess-20-505-2020, publisher: Copernicus GmbH, 2020.

Morard, S., Hilbich, C., Mollaret, C., Pellet, C., and Hauck, C.: 20-year permafrost evolution documented through petrophysical joint inver-sion, thermal and soil moisture data, Environmental Research Letters, 19, 074 074, https://doi.org/10.1088/1748-9326/ad5571, publisher: IOP Publishing, 2024.

745 Noetzli, J., Isaksen, K., Barnett, J., Christiansen, H. H., Delaloye, R., Etzelmüller, B., Farinotti, D., Gallemann, T., Guglielmin, M., Hauck, C., Hilbich, C., Hoelzle, M., Lambiel, C., Magnin, F., Oliva, M., Paro, L., Pogliotti, P., Riedl, C., Schoeneich, P., Valt, M., Vieli, A., and Phillips, M.: Enhanced warming of European mountain permafrost in the early 21st century, Nature Communications, 15, 10 508, https://doi.org/10.1038/s41467-024-54831-9, publisher: Nature Publishing Group, 2024.

Olefs, M. and Lehning, M.: Textile protection of snow and ice: Measured and simulated effects on the energy and mass balance, Cold Regions
750 Science and Technology, 62, 126–141, https://doi.org/10.1016/j.coldregions.2010.03.011, 2010.

Olson, M. and Rupper, S.: Impacts of topographic shading on direct solar radiation for valley glaciers in complex topography, The Cryosphere, 13, 29–40, https://doi.org/10.5194/tc-13-29-2019, publisher: Copernicus GmbH, 2019.

OpenStreetMap contributors: Planet dump retrieved from https://planet.osm.org , https://www.openstreetmap.org, accessed June 17, 2025.

Pellet, C., Hilbich, C., Marmy, A., and Hauck, C.: Soil Moisture Data for the Validation of Permafrost Models Using Direct and Indirect
755 Measurement Approaches at Three Alpine Sites, Frontiers in Earth Science, 3, https://doi.org/10.3389/feart.2015.00091, 2016.

Phillips, M., Ladner, F., Müller, M., Sambeth, U., Sorg, J., and Teysseire, P.: Monitoring and reconstruction of a chair-lift midway station in creeping permafrost terrain, Grächen, Swiss Alps, Cold Regions Science and Technology, 47, 32–42, https://doi.org/10.1016/j.coldregions.2006.08.014, 2007.

Pruessner, L., Phillips, M., Farinotti, D., Hoelzle, M., and Lehning, M.: Near-surface ventilation as a key for modeling the thermal regime of coarse blocky rock glaciers, Permafrost and Periglacial Processes, 29, 152–163, https://doi.org/10.1002/ppp.1978, _eprint: https://onlinelibrary.wiley.com/doi/pdf/10.1002/ppp.1978, 2018.

Pruessner, L., Huss, M., Phillips, M., and Farinotti, D.: A Framework for Modeling Rock Glaciers and Permafrost at the Basin-Scale in High Alpine Catchments, Journal of Advances in Modeling Earth Systems, 13, https://doi.org/10.1029/2020MS002361, 2021.

QGIS Development Team: QGIS Geographic Information System, https://qgis.org, version 3.34.4-Prizren. Available at https://qgis.org, 2023.

Qin, Y., Li, Y., and Bao, T.: An experimental study of reflective shading devices for cooling roadbeds in permafrost regions, Solar Energy, 205, 135–141, https://doi.org/10.1016/j.solener.2020.05.054, 2020.

Qiu, T., Wang, G., Xu, Q., and Ni, G.: Study on the thermal performance and design method of solar reflective–thermal insulation hybrid system for wall and roof in Shanghai, Solar Energy, 171, 851–862, https://doi.org/10.1016/j.solener.2018.07.036, 2018.

Quinton, W., Hayashi, M., and Chasmer, L.: Permafrost-thaw-induced land-cover change in the Canadian subarctic: implications for water resources, Hydrological Processes, 25, 152–158, https://doi.org/10.1002/hyp.7894, _eprint: https://onlinelibrary.wiley.com/doi/pdf/10.1002/hyp.7894, 2011.

Ramamurthy, P., Sun, T., Rule, K., and Bou-Zeid, E.: The joint influence of albedo and insulation on roof performance: A modeling study, Energy and Buildings, 102, 317–327, https://doi.org/10.1016/j.enbuild.2015.06.005, 2015.

Schaefer, K., Lantuit, H., Romanovsky, V. E., Schuur, E. A. G., and Witt, R.: The impact of the permafrost carbon feedback on global climate, Environmental Research Letters, 9, 085 003, https://doi.org/10.1088/1748-9326/9/8/085003, publisher: IOP Publishing, 2014.

Scherler, M., Hauck, C., Hoelzle, M., Stähli, M., and Völksch, I.: Meltwater infiltration into the frozen active layer at an alpine permafrost site, Permafrost and Periglacial Processes, pp. 325–334, https://doi.org/10.1002/ppp.694, 2010.

Schlögl, S., Lehning, M., Nishimura, K., Huwald, H., Cullen, N. J., and Mott, R.: How do Stability Corrections Perform in the Stable Boundary Layer Over Snow?, Boundary-Layer Meteorology, 165, 161–180, https://doi.org/10.1007/s10546-017-0262-1, 2017.

Schmucki, E., Marty, C., Fierz, C., and Lehning, M.: Evaluation of modelled snow depth and snow water equivalent at three contrasting sites in Switzerland using SNOWPACK simulations driven by different meteorological data input, Cold Regions Science and Technology, 99, 27–37, https://doi.org/10.1016/j.coldregions.2013.12.004, 2014.

Sharaborova, E., Loktionov, E., and Shepitko, T.: Method for thermally stabilizing permafrost soils, patent WO/2022/075889, WIPO, 2022a.

Sharaborova, E. S. and Loktionov, E. Y.: SOIL THERMAL STABILIZATION METHOD DUE TO YEAR-ROUND REGULATION OF HEAT TRANSFER, patent RU 2 779 706 C1, 2022.

Sharaborova, E. S., Shepitko, T. V., and Loktionov, E. Y.: Experimental Proof of a Solar-Powered Heat Pump System for Soil Thermal Stabilization, Energies, 15, 2118, https://doi.org/10.3390/en15062118, number: 6 Publisher: Multidisciplinary Digital Publishing Institute, 2022b.

Smith, S. L., O'Neill, H. B., Isaksen, K., Noetzli, J., and Romanovsky, V. E.: The changing thermal state of permafrost, Nature Reviews Earth & Environment, 3, 10–23, https://doi.org/10.1038/s43017-021-00240-1, number: 1 Publisher: Nature Publishing Group, 2022.

Solargis: Global Horizontal Irradiation Switzerland, The World Bank, Source: Global Solar Atlas 2.0, Solar resource data: Solargis, https://solargis.com/maps-and-gis-data/download/switzerland, 2020.

Strand, S. M., Christiansen, H. H., Johansson, M., Åkerman, J., and Humlum, O.: Active layer thickening and controls on interannual variability in the Nordic Arctic compared to the circum-Arctic, Permafrost and Periglacial Processes, 32, 47–58, https://doi.org/https://doi.org/10.1002/ppp.2088, 2021.

Swiss Permafrost Monitoring Network (PERMOS): Swiss Permafrost Monitoring Network Database (PERMOS Database), https://doi.org/10.13093/permos-2024-01, data format: ASCII text, zipped; Data size: 38 MB; Spatial coverage: Swiss Alps, Lat (45.9,46.8), Lon (6.8,10.0); Temporal coverage: 1987 to 2023-09-30; Instruments: thermistor chains, miniature temperature loggers, electrical resistivity tomography, dGPS, total station, 2024.

Swiss Permafrost Monitoring Network (PERMOS) and Hoelzle, M.: Energy balance measurements at three PERMOS sites: Corvatsch, Schilthorn, Stockhorn, https://doi.org/10.13093/permos-meteo-2021-01, 2021.

Tian, Y., Yang, Z., Liu, Y., Cai, X., and Shen, Y.: Long-term thermal stability and settlement of heat pipe-protected highway embankment in warm permafrost regions, Engineering Geology, 292, 106 269, https://doi.org/https://doi.org/10.1016/j.enggeo.2021.106269, 2021.

Wagner, F. M., Mollaret, C., Günther, T., Kemna, A., and Hauck, C.: Quantitative imaging of water, ice and air in permafrost systems through petrophysical joint inversion of seismic refraction and electrical resistivity data, Geophysical Journal International, 219, 1866–1875, https://doi.org/10.1093/gji/ggz402, 2019.

Walter, F., Amann, F., Kos, A., Kenner, R., Phillips, M., de Preux, A., Huss, M., Tognacca, C., Clinton, J., Diehl, T., and Bonanomi, Y.: Direct observations of a three million cubic meter rock-slope collapse with almost immediate initiation of ensuing debris flows, Geomorphology, 351, 106 933, https://doi.org/10.1016/j.geomorph.2019.106933, 2020.

Wang, P., Huang, Q., Tang, Q., Chen, X., Yu, J., Pozdniakov, S. P., and Wang, T.: Increasing annual and extreme precipitation in permafrost-dominated Siberia during 1959–2018, Journal of Hydrology, 603, 126 865, https://doi.org/10.1016/j.jhydrol.2021.126865, 2021.

Wang, Z., Kim, Y., Seo, H., Um, M.-J., and Mao, J.: Permafrost response to vegetation greenness variation in the Arctic tundra through positive feedback in surface air temperature and snow cover, Environmental Research Letters, 14, 044 024, https://doi.org/10.1088/1748-9326/ab0839, publisher: IOP Publishing, 2019.

Weber, S., Beutel, J., Faillettaz, J., Hasler, A., Krautblatter, M., and Vieli, A.: Quantifying irreversible movement in steep, fractured bedrock permafrost on Matterhorn (CH), The Cryosphere, 11, 567–583, https://doi.org/10.5194/tc-11-567-2017, 2017.

Westermann, S., Ingeman-Nielsen, T., Scheer, J., Aalstad, K., Aga, J., Chaudhary, N., Etzelmüller, B., Filhol, S., Kääb, A., Renette, C., Schmidt, L. S., Schuler, T. V., Zweigel, R. B., Martin, L., Morard, S., Ben-Asher, M., Angelopoulos, M., Boike, J., Groenke, B., Miesner, F., Nitzbon, J., Overduin, P., Stuenzi, S. M., and Langer, M.: The CryoGrid community model (version 1.0) – a multi-physics toolbox for climate-driven simulations in the terrestrial cryosphere, Geoscientific Model Development, 16, 2607–2647, https://doi.org/10.5194/gmd-16-2607-2023, publisher: Copernicus GmbH, 2023.

Wever, N., Fierz, C., Mitterer, C., Hirashima, H., and Lehning, M.: Solving Richards Equation for snow improves snowpack meltwater runoff estimations in detailed multi-layer snowpack model, The Cryosphere, 8, 257–274, https://doi.org/10.5194/tc-8-257-2014, 2014.

Wever, N., Schmid, L., Heilig, A., Eisen, O., Fierz, C., and Lehning, M.: Verification of the multi-layer SNOWPACK model with different water transport schemes, The Cryosphere, 9, 2271–2293, https://doi.org/10.5194/tc-9-2271-2015, 2015.

Yinfei, D., Shengyue, W., Shuangjie, W., and Jianbing, C.: Cooling permafrost embankment by enhancing oriented heat conduction in asphalt pavement, Applied Thermal Engineering, 103, 305–313, https://doi.org/10.1016/j.applthermaleng.2016.04.115, 2016.

Zappone, A. and Kissling, E.: SAPHYR: Swiss Atlas of Physical Properties of Rocks: the continental crust in a database, Swiss Journal of Geosciences, 114, 13, https://doi.org/10.1186/s00015-021-00389-3, 2021.

830 Zhang, M., Pei, W., Lai, Y., Niu, F., and Li, S.: Numerical study of the thermal characteristics of a shallow tunnel section with a two-phase closed thermosyphon group in a permafrost region under climate warming, International Journal of Heat and Mass Transfer, 104, 952–963, https://doi.org/10.1016/j.ijheatmasstransfer.2016.09.010, 2017.

Zhao, Y. and Yang, Z. J.: Historical and long-term climate trends in warm permafrost regions: A case study of Bethel, AK, Cold Regions Science and Technology, 204, 103 677, https://doi.org/10.1016/j.coldregions.2022.103677, 2022.

835 Zhu, X., Wu, T., Li, R., Xie, C., Hu, G., Qin, Y., Wang, W., Hao, J., Yang, S., Ni, J., and Yang, C.: Impacts of Summer Extreme Precipitation Events on the Hydrothermal Dynamics of the Active Layer in the Tanggula Permafrost Region on the Qinghai-Tibetan Plateau, Journal of Geophysical Research: Atmospheres, 122, 11,549–11,567, https://doi.org/10.1002/2017JD026736, _eprint: https://onlinelibrary.wiley.com/doi/pdf/10.1002/2017JD026736, 2017.